DMD Fast Forward. Published on January 12, 2018 as DOI: 10.1124/dmd.117.078790
This article has not been copyedited and formatted. The final version may differ from this version.

A study on pharmacokinetics of bosentan with systems modeling, Part 1: translating systemic plasma concentration to liver exposure in healthy subjects

Rui Li, Mark Niosi, Nathaniel Johnson, David A. Tess, Emi Kimoto, Jian Lin, Xin Yang, Keith A. Riccardi, Sangwoo Ryu, Ayman F. El-Kattan, Tristan S. Maurer, Larry M. Tremaine, and Li Di

Systems Modeling and Simulation, Medicine Design, Pfizer Worldwide R&D, Cambridge, MA (RL, DAT, TSM); Pharmacokinetics, Dynamics and Metabolism, Medicine Design, Pfizer Worldwide R&D, Groton, CT (MN, NJ, EK, JL, XY, KAR, SR, LMT, LD); Pharmacokinetics, Dynamics and Metabolism, Medicine Design, Pfizer Worldwide R&D, Cambridge, MA (AFE).

Running title

Translating bosentan systemic exposure to liver exposure

Corresponding Author

Rui Li. Systems Modeling and Simulation, Medicine Design, Pfizer Worldwide R&D, Cambridge, MA. Phone: 617-551-3340. Email: Rui.Li5@pfizer.com

Number of text pages: 12

Number of tables: 4

Number of Figures: 7

Number of references: 34

Number of words in Abstract: 178

Number of words in Introduction: 627

Number of words in Discussion: 1331

DMD Fast Forward. Published on January 12, 2018 as DOI: 10.1124/dmd.117.078790
This article has not been copyedited and formatted. The final version may differ from this version.

Abbreviations

BSEP: bile salt export pump

CYP: cytochrome P450

DDI: drug-drug interaction

DILI: drug-induced liver injury

ECCS: Extended Clearance Classification System

ET: endothelin receptors,

Kp_{uu}: unbound tissue-to-unbound systemic plasma concentration ratio

Kp_{u}: total tissue-to-unbound systemic plasma concentration ratio

MCMC: Markov chain Monte Carlo

MRP: multidrug resistance-associated protein

NTCP: sodium-taurocholate co-transporting polypeptide

OATP: organic anion transporting polypeptide

PBPK: physiologically based pharmacokinetic

PD: pharmacodynamics

PET: positron emission tomography

PK: pharmacokinetics

PXR: pregnane X receptor

RBC: red blood cells

SCHH: sandwich cultured human hepatocyte

TMDD: target mediated drug disposition

UGT: UDP-glucuronosyltransferase

Abstract

Understanding liver exposure of hepatic transporter substrates in clinical studies is often critical as it typically governs pharmacodynamics, drug-drug interactions, and toxicity for certain drugs. However, this is a challenging task since there is currently no easy method to directly measure drug concentration in the human liver. Using bosentan as an example, a new approach has been demonstrated to estimate liver exposure based on observed systemic pharmacokinetics from clinical studies using physiologically-based pharmacokinetic modeling. The prediction has been verified to be both accurate and precise using sensitivity analysis. For bosentan, the predicted pseudo steady state unbound liver-to-unbound systemic plasma concentration ratio (Kp_{uu}) is 34.9 with a 95% confidence interval of 4.2 to 50. Drug-drug interaction (i.e., cytochrome P450 (CYP) 3A and 2B6 induction) and inhibition of hepatic transporter (i.e., bile salt export pump (BSEP), multidrug resistance-associated proteins (MRPs), and sodium-taurocholate co-transporting polypeptide (NTCP)) are predicted based on the estimated unbound liver tissue or plasma concentrations. With further validation and refinement, it is concluded that the approach may serve to predict human liver exposure and complement other methods involving tissue biopsy and imaging.

Introduction

The pharmacokinetics (PK) of many drugs can be influenced by transporters. Since transporter-mediated disposition (e.g., organic anion transporting polypeptides, OATPs) can be independent of substrate concentration gradient, drugs may accumulate or be excluded from tissues. Therefore, even without considering factors like membrane potential, it may not be accurate to assume that unbound tissue concentration is equivalent to unbound plasma concentration (Kp_{uu} = 1). Since both transporters and metabolism affect drug concentration in the liver, there are two challenges for drug discovery: (1) predicting systemic exposure, which is dependent upon the interplay between transporters and metabolism in the liver, and (2) predicting liver exposure, which may drive pharmacodynamics (PD), toxicity, and drug-drug interaction (DDI). In the drug development phase, even with clinical data, predicting liver exposure may still be ambiguous in relating observed plasma PK to tissue-exposure-driven clinical outcomes.

To address the challenge of understanding human liver exposure, positron emission tomography (PET) studies for transporter substrates have been developed (Shimizu et al., 2012; Gormsen et al., 2016). In addition to excessive cost and potential difficulties in labeling compounds, the usefulness of this approach is still limited to compounds with minimal metabolism. For the majority of drugs with significant metabolism, the PET data is confounded by metabolite signals. As such, in the foreseeable future, translating observed systemic concentration to liver concentration with mechanistic modeling (e.g., physiologically based pharmacokinetic, PBPK models) may be one of the most effective tools to enable a greater understanding of human liver exposure. However, this approach has its limitations, including non-ideal systemic data making the PBPK model unidentifiable, so that many sets of parameter values can equally describe the systemic plasma data, but lead to different liver exposure predictions (Li et al., 2016).

From such a perspective, bosentan is a great example as its systemic exposure data can provide enough information for PBPK modeling to confidently predict liver concentrations. Bosentan is a dual endothelin receptor antagonist, used to treat pulmonary arterial hypertension (Dingemanse and van Giersbergen, 2004). Being an Extended Clearance Classification System (ECCS) 1B compound (El-Kattan et al., 2016), in human bosentan

is transported into the liver by uptake transporters including OATP1B1 and OATP1B3 (Treiber et al., 2007) and then metabolized by cytochromes P450 (CYP) 3A and 2C9 (Dingemanse and van Giersbergen, 2004), with minimal unchanged drug recovered in urine and feces following intravenous dosing (Weber et al., 1999b). Although the PK profile of bosentan is more complicated than other compounds (e.g., nonlinear disposition and distribution (Weber et al., 1996)), these can be addressed with a carefully calibrated model. Bosentan is not characterized by significant biliary excretion or enterohepatic recirculation, which would have made data interpolation very challenging.

Understanding bosentan liver exposure is also important for predicting CYP induction and inhibition. Several groups have reported that bosentan is an inducer for CYPs (van Giersbergen et al., 2002a; Dingemanse and van Giersbergen, 2004; Fahmi et al., 2008; Srinivas, 2016; Sun et al., 2017). Results of in vitro studies also show that bosentan inhibits the bile salt export pump (BSEP), multidrug resistance-associated protein (MRP) 3 and 4 (Morgan et al., 2013), sodium-taurocholate co-transporting polypeptide (NTCP) (Leslie et al., 2007), which may result in drug-induced liver injury (DILI) (Leslie et al., 2007; Morgan et al., 2013). Hepatic CYP induction and transporter inhibition is likely driven by liver concentration, so a highly confident prediction of liver concentration is critical to understand clinically observed DDI and DILI.

In this study, we have developed a PBPK model for bosentan incorporating its various PK properties, and generated liver exposure and its confidence intervals using a Markov chain Monte Carlo (MCMC) approach. The key parameters are determined either in preclinical assays or by simultaneously fitting data from eight independent clinical studies (Table 1) to avoid potential model misspecifications due to improper assumptions.

Materials and Methods

A mechanistic model to analyze pharmacokinetic data

Framework. A new PBPK model (with scheme in Figure 1) is developed based on a published structure (Li et al., 2014). Table 2 provides all the parameters with fixed values, except for the physiological parameters listed in Supplemental Materials (Supplemental

DMD Fast Forward. Published on January 12, 2018 as DOI: 10.1124/dmd.117.078790
This article has not been copyedited and formatted. The final version may differ from this version.

Table S1). Equations and all other modeling details not covered in the text are presented in Supplemental Materials.

Systemic circulation and non-liver tissue distribution. The arterial blood, venous blood, and lung are lumped as systemic blood, which is then split into systemic plasma and red blood cells (RBC). Due to potential nonlinear binding kinetics, instead of assuming constant plasma unbound fraction ($f_{u,p}$) or blood to plasma ratio ($R_{B/P}$), we use the kinetic model to describe binding in plasma and RBC. For example, binding in the plasma is modeled with mass balances of unbound concentration, bound concentration, and available binding site concentration (Equation 1 to 3)

$$\frac{dC_{unbound}}{dt} = -k_{on} \cdot C_{unbound} \cdot C_{available-site} + k_{off} \cdot C_{bound} \quad (1)$$

$$\frac{dC_{available-site}}{dt} = -k_{on} \cdot C_{unbound} \cdot C_{available-site} + k_{off} \cdot C_{bound} \quad (2)$$

$$\frac{dC_{bound}}{dt} = k_{on} \cdot C_{unbound} \cdot C_{available-site} - k_{off} \cdot C_{bound} \quad (3)$$

The binding in RBC is modeled similarly; passive permeation ($CL_{systemic,blood,pass}$) is assumed between RBC and plasma. All components in the systemic blood are connected with their counterparts in the liver and small intestine villi blood.

k_{on} rates for all binding processes in this study are fixed at 10^9 $mol^{-1} \cdot sec^{-1}$ (3600 $nmol^{-1} \cdot hour^{-1}$) assuming the diffusion limited reaction (Alberty and Hammes, 1958). k_{off} and the total concentrations of binding site in plasma and RBC are estimated by fitting in vitro unbound fraction and blood to plasma ratio at various concentrations (Supplemental Materials Figure S1) with a mechanistic model. As the model is not sensitive to $CL_{systemic,blood,pass}$, this parameter is fixed at the product of total systemic RBC surface area and a permeability approximated using hepatocytes; details provided in Supplemental Materials.

For non-liver tissues, instantaneous equilibrium between tissue and unbound systemic plasma is assumed, defined by in silico predicted Kp_u (i.e., total tissue to unbound plasma

ratio) values (Rodgers and Rowland, 2006). The target mediated drug disposition (TMDD) has been proposed in previous studies (Mager and Jusko, 2001; Volz et al., 2017), but it's unlikely that the targets (i.e., endothelin receptors, ET) or their internalization will eliminate the compound. As such, TMDD is modeled as a specific binding process to the ET in the plasma compartment, with parameters optimized by fitting clinical data.

The liver. The model includes five sequential liver segments, each containing three components: plasma, RBC, and tissue. Each component is further divided into three sub-components to represent unbound, bound compound, and available binding site. There are hepatic active uptake, active basal efflux, and passive diffusion between plasma and tissue, plus metabolism within the tissue. The biliary excretion is assumed to be minimal for bosentan based on the fact that: (1) in vitro sandwich cultured human hepatocyte (SCHH) showed no biliary excretion (data provided in Part 2 of this study, which is published in a separated article), and (2) minimal compound is excreted into feces following intravenous dosing in humans (Weber et al., 1999b). With the exception of passive diffusion clearance ($CL_{liver,pass}$), hepatic processes are assumed to follow Michaelis-Menten kinetics. Among Michaelis-Menten constants, $K_{M,liver,uptake}$ and $K_{M,liver,metabolism}$ are fixed at values based on in vitro assays. Due to low confidence in the in vitro values, $K_{M,liver,efflux}$ is estimated by fitting clinical data, together with $k_{liver,uptake}$, $k_{liver,efflux}$, $k_{liver,metabolism}$ and $CL_{liver,pass}$. Blood binding parameters share the same values as those in circulating blood. Intracellular binding parameters are fixed at values estimated from in vitro hepatocyte assays in Part 2.

Absorption parameters. The oral absorption is modeled using a semi-mechanistic model with a first order rate constant (k_a) and fraction absorbed (F_a). An enterocyte compartment is created between dissolved drug compartment and small intestine villi blood. Passive diffusion ($CL_{enterocyte,pass}$) and active efflux ($CL_{enterocyte,efflux}$) are assumed between enterocytes and small intestine villi blood, and metabolism in the enterocytes. Binding in villi blood is modeled the same as that within systemic and liver blood. Fraction absorbed (F_a) is determined using clinical ^{14}C data (with details provided in Supplemental Materials). Two different k_a values under fasted and fed conditions, $CL_{enterocyte,pass}$, $CL_{enterocyte,efflux}$ and

DMD Fast Forward. Published on January 12, 2018 as DOI: 10.1124/dmd.117.078790
This article has not been copyedited and formatted. The final version may differ from this version.

enterocyte intracellular free fraction ($f_{u,enterocyte}$) are estimated by fitting clinical data. Although apparent K_M values for enterocyte and liver metabolism may be different due to potentially different CYPs involved in the tissues, we assume that $K_{M,enterocyte,metabolism}$ shares the same value with $K_{M,liver,metabolism}$ based upon fact that the in vitro CYP3A- and 2C9 have similar K_M values (Shen et al., 2009), whereas the metabolic rate is scaled from $k_{liver,metabolism}$ based on CYP abundances in the human liver and gut (details provided in Supplemental Materials).

Induction parameters. In vivo CYP induction is described using a turnover model. Because bosentan induces CYPs via pregnane X receptor (PXR) agonism (van Giersbergen et al., 2002a), we assume that different CYPs involved in hepatic and intestinal metabolism share the same induction E_{max} and EC_{50} values, which is supported by the similar values identified from the in vitro CYP3A4 and 2B6 activity assay described below. E_{max} is estimated by fitting clinical data of bosentan and victim drugs (see below), while EC_{50} is fixed at an average value from the in vitro assay (i.e., 1000 nM). CYP degradation rate ($k_{degradatin}$) is calculated as ln(2) divided by half-life. Because there is no published clinical data regarding CYP2C9 half-life, it is assumed that degradation rate ($k_{liver,degradation}$) of CYP2C9 equals that of CYP3A4, estimated from a clinical CYP3A4 inactivation study (27.7 hours (Quinney et al., 2010)). The enterocyte half-life (23.1 hours (Yang et al., 2008)) is applied to enterocyte CYPs, assuming half-life values of CYPs are determined by the shorter half-life of enterocyte.

BSEP, MRP, NTCP inhibition. Competitive inhibition of four transporters was calculated independently based on simulated bosentan unbound plasma (for NTCP) or intracellular (for BSEP and MRP) concentrations and in vitro IC_{50} values (Leslie et al., 2007; Morgan et al., 2013). Maximal inhibition is assumed to be 100%. There is no supporting evidence that inhibition affects bosentan exposure.

DMD Fast Forward. Published on January 12, 2018 as DOI: 10.1124/dmd.117.078790
This article has not been copyedited and formatted. The final version may differ from this version.

Victim drugs. A reduced PBPK model is developed for victim drugs (i.e., tadalafil and warfarin) co-dosed with bosentan (Supplemental Materials). Published bosentan induction DDI studies with other drugs are not included in the modeling since it is challenging to simulate victim liver exposure (e.g., transporter substrates: simvastatin and glyburide) or because victim drugs also affect bosentan exposure (e.g., glyburide reduces bosentan exposure, and sildenafil increases bosentan exposure). For victim drugs, bosentan may change its gut metabolism (F_g), hence we assume that their F_g values are different with and without bosentan. Since it is difficult to separate F_a from fraction escaped from F_g, F_aF_g is modeled as a single parameter. It is fixed at one in the absence of bosentan, but fitted against clinical data in the presence of bosentan. Parameters for victim drugs in the absence of bosentan are listed in Supplemental Table S2.

Parameter optimization and prediction of liver exposure

Bosentan data from eight clinical studies are included for parameter optimization (Table 1). The model is implemented in MATLAB 2016a (MathWorks, Natick, MA, US). Parameter estimation is performed with differential evolution, while the uncertainty is quantified using MCMC (Markov chain Monte Carlo). MCMC provides ranges of parameter values that are able to reasonably describe the data. We randomly sampled 1000 sets of parameter values from all values (8×10^5 sets) identified in MCMC that adequately describe systemic plasma data. 1000 simulations using sampled parameter values were generated, such that uncertainty in parameter estimation was reflected in the simulations.

In vitro induction assay and modeling

An in vitro hepatocyte induction study was performed to understand if the CYP induction could be accurately predicted using primary hepatocytes. The data are analyzed using a mechanistic model which combines SCHH model and CYP turnover model mentioned above. Details are provided in the Supplemental Materials.

Results

DMD Fast Forward. Published on January 12, 2018 as DOI: 10.1124/dmd.117.078790
This article has not been copyedited and formatted. The final version may differ from this version.

Fitting clinical systemic data and estimating parameters

With optimized parameter values, the model can reasonably describe the mean systemic exposures of both bosentan and victim drugs following intravenous or oral administration with various doses (Figure 2, 3, and 4) obtained from several studies. Parameters can be confidently estimated (Table 3) with the exception of $CL_{enterocyte,pass}$, $CL_{enterocyte,efflux}$, $k_{liver,efflux}$, and $K_{M,liver,efflux}$. This is potentially due to correlation among the different parameters, or insensitivity of simulations to these parameters.

Simulating liver exposure

Despite the fact that some parameters cannot be confidently identified by fitting systemic data, the predicted liver exposure is still reasonably precise (Figure 5). The predicted pseudo steady state ratio between unbound liver tissue and unbound systemic plasma concentrations ($Kp_{uu,liver}$, i.e., the ratio during the elimination phase of systemic PK) following 125 mg bosentan BID dosing is 34.9 with 95% confidence interval (CI) of 4.2 and 50. The time course of unbound liver tissue to unbound systemic plasma following 62.5, 125, or 500 mg BID dosing are provided in Figure 5 (B, E, and H), where the median values change between 20 and 40. Please note that $Kp_{uu,liver}$ calculated here is the ratio of unbound liver tissue to unbound systemic plasma concentration, but not to unbound liver plasma concentration. Hypothetically, there is a difference in concentration between systemic plasma and liver plasma due to liver extraction.

CYP induction

With the data included in this study, a liver induction effect of around 1.5-fold and a gut induction effect of about 2-fold are estimated, depending on the dosing amounts (Figure 5C, F, and I). The result is consistent with a previous clinical study where bosentan increases the urinary excretion of 6β-hydroxycortisol (an endogenous marker of CYP3A4 activity) 1.7-fold (Weber et al., 1999c). Following 125 mg twice daily oral dosing for ten days, using metabolic rate estimated in MCMC, bosentan F_g is calculated to be 0.630 (95% CI: 0.57, 0.68) during the first dose, and 0.473 (95% CI: 0.41, 0.53) during the last dose.

DMD Fast Forward. Published on January 12, 2018 as DOI: 10.1124/dmd.117.078790
This article has not been copyedited and formatted. The final version may differ from this version.

The ratio between two F_g is 0.751 (95% CI: 0.70, 0.81). Overall, the model attributes more induction effect to gut rather than liver, which is similar to a previous results published for DDI between repaglinide and rifampin (Varma et al., 2013). Since tadalafil absolute bioavailability is unknown, and we arbitrarily assume its F_aF_g to be 1 in the absence of bosentan, the estimated F_aF_g in the presence of bosentan (Table 3) is essentially the ratio of F_aF_g between two conditions. Further assuming its F_a is not affected by bosentan, its F_g in the presence of bosentan is reduced to 0.868 (95% CI: 0.70, 1.0) of F_g value in the absence of bosentan. This is consistent with bosentan F_g changes described above. For warfarin, this ratio is around 1 (Table 3). This is consistent with the fact that warfarin bioavailability (and hence F_g) is nearly 1 (Holford, 1986) (i.e., warfarin has minimal gut metabolism).

We have also generated in vitro CYP3A and 2B6 induction data using human hepatocytes (Table 4, Supplemental Figure S2) to understand the prediction accuracy of the current in vitro tool. By measuring activity, prediction from lot HH1025 is closest to the in vivo simulations, while the other two lots (i.e. HC7-4 and FOS) would over-predict in vivo induction (Figure 6). By measuring mRNA, the assay over-predicts observed induction based on clinical data, which is consistent with another CYP inducer, rifampin (in-house data not shown).

BSEP, MRP, NTCP inhibition

With the predicted unbound liver tissue or plasma exposure and published IC_{50} values estimated from in vitro data, the model predicts moderate inhibition (up to 18%) for these transporters (Figure 7).

Discussion

This study aims to predict the liver concentration of a transporter substrate by leveraging a PBPK model that utilizes available clinical (systemic plasma concentration) data. The underlying mechanism for such a prediction is the conservation of mass: the total amount of the compound in systemic blood, liver, non-liver tissues, and the compound metabolized

DMD Fast Forward. Published on January 12, 2018 as DOI: 10.1124/dmd.117.078790
This article has not been copyedited and formatted. The final version may differ from this version.

is equal to the dosed amount. In such a scenario, the dosed amount is known. The amount in systemic blood is based on measured plasma concentrations, amount in non-liver tissue is predicted with in silico methods, and the amount metabolized can be calculated using hepatic metabolic rate estimated from systemic data. As a result, the amount in the liver can be deduced. A precise and accurate "deduction" is based upon three criteria. First, the model's ability to accurately describe systemic data (amount in systemic blood) is a prerequisite for predicting liver concentration, which explains why we establish this relatively complex PBPK model incorporating multiple nonlinear processes. Second, there must be sufficient data to enable confident estimation of hepatic metabolism. For certain compounds, their clinical data cannot satisfy this requirement as described previously (Li et al., 2016). With a MCMC approach, we have shown that bosentan metabolism can be precisely estimated from its clinical systemic data. Third, an accurate description of distribution into non-liver tissues is critical, which is usually predicted by the in silico estimated Kp_u values in human PBPK modeling. To understand how inaccurate non-liver Kp_u (distribution into non-liver tissues) may affect liver Kp_{uu} estimation, we have applied a scaler for non-liver Kp_u at the value of 0.1 or 10, and re-estimated liver Kp_{uu}. With a non-liver Kp_u scaler of 0.1, the goodness of fitting of the systemic data is about the same as that without using a scaler, and liver Kp_{uu} is about 40. The latter is still within the confidence interval of liver Kp_{uu} without non-liver Kp_u scaler. On the other hand, with a non-liver Kp_u scaler of 10, the goodness of fitting is significantly worse (i.e. objective function value increased by 5 fold), and the liver Kp_{uu} cannot be confidently identified. We have also tried to estimate a Kp_u scaler by including it as another fitted parameter; however, this parameter cannot be precisely estimated. In a monkey study presented in Part 2 of this work, where both systemic and liver exposure are determined experimentally, we can confidently estimate the non-liver Kp_u scaler as 1.47, which justifies a value of 1 in the present exercise.

Binding to bosentan's pharmacology target may also affect distribution. The ratio, K_D, between ET k_{off} and k_{on} is estimated to be 4.30 (with 95% CI between 1.4 and 11), which is very close to experimentally determined values (Russell and Davenport, 1995; Bacon and Davenport, 1996; Gatfield et al., 2012). Although we set these parameters for ET binding, the optimization process may also use them to describe tissue distribution not explained by tissue Kp_u fixed at the in silico predicted values. The fact that the estimated

DMD Fast Forward. Published on January 12, 2018 as DOI: 10.1124/dmd.117.078790
This article has not been copyedited and formatted. The final version may differ from this version.

K_D value is similar to experimentally determined values suggests non-liver Kp_u used in the model is likely accurate. Alternatively, if non-liver Kp_u was inaccurate, the model would likely incorrectly estimate ET K_D.

Bosentan is mostly metabolized by CYP3A with a minor contribution from CYP2C9 (70% versus 10%, supplemental materials). For the induction victim drugs, tadalafil is primarily metabolized by CYP3A (Wrishko et al., 2008), CYP3A contributes to (R)-warfarin clearance, and (S)-warfarin is largely metabolized by CYP2C9 (Weber et al., 1999a). To reduce the number of fitted parameters, we assume that different CYPs share the same induction E_{max} and EC_{50}, based on the fact that bosentan induces CYP via PXR-mediated mechanisms. It is difficult to validate this assumption without additional clinical data. Because the estimated hepatic induction effect is minimal, the specific values for each hepatic CYP are unlikely to significantly affect current simulations. For enterocyte induction in the gut, which is stronger than hepatic induction, we assume that induction is compound-specific. Nonetheless, we have also re-estimated liver Kp_{uu} after removing data from victim drugs. Neither estimated parameter values nor Kp_{uu} changes significantly. As a result, even if the future data show that assumption made here for hepatic induction E_{max} and EC_{50} is incorrect, it should not significantly confound the liver simulations. It is worth noting that simulated induction effect (Figure 5C, F, and I) is consistent with the result of a previous clinical study where an endogenous marker of CYP3A4 activity was monitored. In addition, estimated changes of F_g values due to induction are similar between bosentan and tadalafil. These results are consistent with the fact that bosentan and tadalafil are mostly metabolized by CYP3A.

An average of 10% transporter inhibition is predicted, but the PBPK model does not include bosentan metabolites, which may lead to more inhibition. However, it is out of scope of the current study to determine how much inhibition is required to cause DILI.

To increase confidence in the simulations, the model is trained with data collected from several clinical studies. Although intravenous bolus studies are generally excluded from first-in-human studies due to the cost of developing formulation, safety concerns, etc. It may, however, be a cost effective way to understand liver exposure (i.e., exposure at the site of action) compared to other approaches, such as PET, which can be difficult to

interpret due to metabolite interference. We therefore recommend human intravenous bolus studies collecting data in both distribution and terminal phases for future clinical trials to provide a greater understanding of liver exposure for compounds undergoing metabolism. With only oral data, there are additional fitted absorption parameters which may lead to over-parameterization. Oral studies may be acceptable for compounds with known F_aF_g. Failure in collecting data in terminal phase may add uncertainty in identifying hepatic metabolism and liver exposure. If parameters cannot be confidently estimated even with intravenous data, the Bayesian based approaches may have to be used with the risk of using inaccurate priors. For compounds with minimal metabolism but extensive biliary excretion and enterohepatic recirculation, PBPK modeling is restricted by our limited understanding of elimination mechanisms, whereas PET studies may provide more straightforward results. For compounds with both metabolism and enterohepatic recirculation (e.g., UDP-glucuronosyltransferase, UGT substrates), we cannot see any clinical approach beneficial in understanding their liver exposures so far.

Yoshikado et al. reported that a generally accepted CYP3A inhibitor, itraconazole, did not significantly change bosentan systemic exposure in human (Yoshikado et al., 2017). The authors estimated in vivo CYP3A inhibition by itraconazole using orally administered midazolam as a victim compound (where plasma AUC ratio was 3.7), and assumed that itraconazole could inhibit bosentan metabolism to the same level. The fact that itraconazole did not change bosentan systemic exposure led the authors to conclude that the ratio of hepatic metabolism to passive diffusion was high, such that the change of metabolism within the liver was not reflected in systemic exposure. This conclusion contradicts our parameter estimation, where passive diffusion is high enough so CYP3A inhibition will change systemic exposure (simulation not shown). It worth noting that in the Yoshikado study, itraconazole did not significantly change bosentan metabolite exposure either. It is possible that itraconazole cannot sufficiently inhibit bosentan metabolism under in vivo conditions, hence it would not affect bosentan systemic exposure, independent of bosentan's permeability. In addition, a second CYP3A inhibitor, ketoconazole, has been shown to significantly alter bosentan systemic exposure (van Giersbergen et al., 2002b), which is consistent with our prediction.

In conclusion, using bosentan data, we have provided an example to demonstrate how to translate the systemic concentration of a hepatic transporter substrate into its liver exposure by leveraging a PBPK based “deduction” method. The precision and accuracy of such a translation has been evaluated and discussed also. As described, the new approach supports determination of drug liver exposure in humans based on existing clinical data, as information regarding the exposure at the site of action is critical for hepatic transporter substrates when attempting to understand their PD, DDI, toxicity in the liver, and therapeutic index.

Acknowledgments

We thank Drs. David Rodrigues and Theunis Goosen (Pfizer Inc.) for helpful discussions, and Ms. Karen Atkinson (Pfizer Inc.) for assistance with manuscript editing.

Authorship Contributions

Participated in research design: Li, Niosi, Tess, Lin, El-Kattan, Maurer, Tremaine, and Di.

Conducted experiments: Niosi, Johnson, Kimoto, Yang, Riccardi, Ryn.

Contributed new reagents or analytic tools: Li.

Performed data analysis: Li, Niosi, Johnson, Kimoto, Tess, Tremaine, and Di

Wrote or contributed to the writing of the manuscript: Li, Johnson, and Di

References

Alberty RA and Hammes GG (1958) Application of the Theory of Diffusion-controlled Reactions to Enzyme Kinetics. *The Journal of Physical Chemistry* **62:**154-159.

Bacon CR and Davenport AP (1996) Endothelin receptors in human coronary artery and aorta. *Br J Pharmacol* **117:**986-992.

Dingemanse J, Bodin F, Weidekamm E, Kutz K, and van Giersbergen P (2002) Influence of food intake and formulation on the pharmacokinetics and metabolism of bosentan, a dual endothelin receptor antagonist. *J Clin Pharmacol* **42:**283-289.

Dingemanse J and van Giersbergen PL (2004) Clinical pharmacology of bosentan, a dual endothelin receptor antagonist. *Clin Pharmacokinet* **43:**1089-1115.

El-Kattan AF, Varma MV, Steyn SJ, Scott DO, Maurer TS, and Bergman A (2016) Projecting ADME Behavior and Drug-Drug Interactions in Early Discovery and Development: Application of the Extended Clearance Classification System. *Pharm Res* **33:**3021-3030.

Fahmi OA, Maurer TS, Kish M, Cardenas E, Boldt S, and Nettleton D (2008) A combined model for predicting CYP3A4 clinical net drug-drug interaction based on CYP3A4 inhibition, inactivation, and induction determined in vitro. *Drug Metab Dispos* **36:**1698-1708.

Gatfield J, Mueller Grandjean C, Sasse T, Clozel M, and Nayler O (2012) Slow receptor dissociation kinetics differentiate macitentan from other endothelin receptor antagonists in pulmonary arterial smooth muscle cells. *PLoS One* **7:**e47662.

Gormsen LC, Sundelin EI, Jensen JB, Vendelbo MH, Jakobsen S, Munk OL, Hougaard Christensen MM, Brosen K, Frokiaer J, and Jessen N (2016) In Vivo Imaging of Human 11C-Metformin in Peripheral Organs: Dosimetry, Biodistribution, and Kinetic Analyses. *J Nucl Med* **57:**1920-1926.

Holford NHG (1986) Clinical Pharmacokinetics and Pharmacodynamics of Warfarin. *Clinical Pharmacokinetics* **11:**483-504.

Leslie EM, Watkins PB, Kim RB, and Brouwer KL (2007) Differential inhibition of rat and human Na+-dependent taurocholate cotransporting polypeptide (NTCP/SLC10A1)by bosentan: a mechanism for species differences in hepatotoxicity. *J Pharmacol Exp Ther* **321:**1170-1178.

Li R, Barton HA, Yates PD, Ghosh A, Wolford AC, Riccardi KA, and Maurer TS (2014) A "middle-out" approach to human pharmacokinetic predictions for OATP substrates using physiologically-based pharmacokinetic modeling. *J Pharmacokinet Pharmacodyn* **41:**197-209.

Li R, Maurer TS, Sweeney K, and Barton HA (2016) Does the Systemic Plasma Profile Inform the Liver Profile? Analysis Using a Physiologically Based Pharmacokinetic Model and Individual Compounds. *The AAPS Journal* **18:**746-756.

Mager DE and Jusko WJ (2001) General pharmacokinetic model for drugs exhibiting target-mediated drug disposition. *J Pharmacokinet Pharmacodyn* **28:**507-532.

Morgan RE, van Staden CJ, Chen Y, Kalyanaraman N, Kalanzi J, Dunn RT, 2nd, Afshari CA, and Hamadeh HK (2013) A multifactorial approach to hepatobiliary transporter assessment enables improved therapeutic compound development. *Toxicol Sci* **136:**216-241.

NDA-21-290 (2001) Clinical pharmacology and biopharmaceutics review. *Center for Drug Devaluation and Research, US Food and Drug Administration*.

Quinney SK, Zhang X, Lucksiri A, Gorski JC, Li L, and Hall SD (2010) Physiologically based pharmacokinetic model of mechanism-based inhibition of CYP3A by clarithromycin. *Drug Metab Dispos* **38:**241-248.

Rodgers T and Rowland M (2006) Physiologically based pharmacokinetic modelling 2: predicting the tissue distribution of acids, very weak bases, neutrals and zwitterions. *J Pharm Sci* **95:**1238-1257.

Russell FD and Davenport AP (1995) Characterization of Endothelin Receptors in the Human Pulmonary Vasculature Using Bosentan, SB209670, and 97-139. *Journal of Cardiovascular Pharmacology* **26:**S346-347.

Shen G, Yao M, Fura A, and Zhu M (2009) In vitro metabolite identification and cytochrome P450 reaction phenotyping of Bosentan, a dual endothelin receptor antagonist, in: *AAPS Annual Meeting and Exposition*, Los Angeles, CA, US.

Shimizu K, Takashima T, Yamane T, Sasaki M, Kageyama H, Hashizume Y, Maeda K, Sugiyama Y, Watanabe Y, and Senda M (2012) Whole-body distribution and radiation dosimetry of [11C]telmisartan as a biomarker for hepatic organic anion transporting polypeptide (OATP) 1B3. *Nucl Med Biol* **39:**847-853.

Srinivas NR (2016) Clinical drug-drug interactions of bosentan, a potent endothelial receptor antagonist, with various drugs: Physiological role of enzymes and transporters. *Gen Physiol Biophys* **35:**243-258.

Sun Y, Chothe PP, Sager J, Tsao H, Moore A, Laitinen L, and Hariparsad N (2017) Quantitative Prediction of CYP3A4 Induction: Impact of Measured, Free and Intracellular Perpetrator Concentrations from Human Hepatocyte Induction Studies on Drug-Drug Interaction Predictions. *Drug Metab Dispos*.

Treiber A, Schneiter R, Häusler S, and Stieger B (2007) Bosentan Is a Substrate of Human OATP1B1 and OATP1B3: Inhibition of Hepatic Uptake as the Common Mechanism of Its Interactions with Cyclosporin A, Rifampicin, and Sildenafil. *Drug Metabolism and Disposition* **35:**1400-1407.

van Giersbergen PL, Gnerre C, Treiber A, Dingemanse J, and Meyer UA (2002a) Bosentan, a dual endothelin receptor antagonist, activates the pregnane X nuclear receptor. *Eur J Pharmacol* **450:**115-121.

van Giersbergen PL, Halabi A, and Dingemanse J (2002b) Single- and multiple-dose pharmacokinetics of bosentan and its interaction with ketoconazole. *Br J Clin Pharmacol* **53:**589-595.

Varma MV, Lin J, Bi YA, Rotter CJ, Fahmi OA, Lam JL, El-Kattan AF, Goosen TC, and Lai Y (2013) Quantitative prediction of repaglinide-rifampicin complex drug interactions using dynamic and static mechanistic models: delineating differential CYP3A4 induction and OATP1B1 inhibition potential of rifampicin. *Drug Metab Dispos* **41:**966-974.

Volz AK, Krause A, Haefeli WE, Dingemanse J, and Lehr T (2017) Target-Mediated Drug Disposition Pharmacokinetic-Pharmacodynamic Model of Bosentan and Endothelin-1. *Clin Pharmacokinet*.

Weber C, Banken L, Birnboeck H, and Schulz R (1999a) Effect of the endothelin-receptor antagonist bosentan on the pharmacokinetics and pharmacodynamics of warfarin. *J Clin Pharmacol* **39:**847-854.

Weber C, Gasser R, and Hopfgartner G (1999b) Absorption, excretion, and metabolism of the endothelin receptor antagonist bosentan in healthy male subjects. *Drug Metab Dispos* **27:**810-815.

Weber C, Schmitt R, Birnboeck H, Hopfgartner G, Eggers H, Meyer J, van Marle S, Viischer HW, and Jonkman JH (1999c) Multiple-dose pharmacokinetics, safety, and tolerability of bosentan, an endothelin receptor antagonist, in healthy male volunteers. *J Clin Pharmacol* **39:**703-714.

Weber C, Schmitt R, Birnboeck H, Hopfgartner G, van Marle SP, Peeters PA, Jonkman JH, and Jones CR (1996) Pharmacokinetics and pharmacodynamics of the endothelin-receptor antagonist bosentan in healthy human subjects. *Clin Pharmacol Ther* **60:**124-137.

Wrishko RE, Dingemanse J, Yu A, Darstein C, Phillips DL, and Mitchell MI (2008) Pharmacokinetic Interaction Between Tadalafil and Bosentan in Healthy Male Subjects. *The Journal of Clinical Pharmacology* **48:**610-618.

Yang J, Liao M, Shou M, Jamei M, Yeo KR, Tucker GT, and Rostami-Hodjegan A (2008) Cytochrome p450 turnover: regulation of synthesis and degradation, methods for determining rates, and implications for the prediction of drug interactions. *Curr Drug Metab* **9:**384-394.

Yoshikado T, Maeda K, Furihata S, Terashima H, Nakayama T, Ishigame K, Tsunemoto K, Kusuhara H, Furihata KI, and Sugiyama Y (2017) A Clinical Cassette Dosing Study for Evaluating the Contribution of Hepatic OATPs and CYP3A to Drug-Drug Interactions. *Pharm Res* **34:**1570-1583.

Figure Captions

Figure 1. Schematic diagram of a PBPK model for bosentan. Only two liver segments are presented in this scheme, but there are five segments in the model. Non-liver tissue type II represents tissues whose venous blood enters portal vein, while type I represents the rest non-liver tissues.

Figure 2. Observed (circles) and simulated (solid lines) total systemic plasma concentrations of bosentan following intravenous dosing.

Figure 3. Observed (circles) and simulated (solid lines) total systemic plasma concentrations of bosentan following oral dosing. Subplots (A) to (F) show the multiple oral dosing with different amounts. Subplots (G) and (H) show the single oral dosing with high fat meal.

Figure 4. Observed (circles) and simulated (solid lines) total systemic plasma concentrations of tadalafil on day 1 (A and B), day 10 (C and D), S-warfarin (E and F), and R-warfarin (G and H). Subplots (A), (C), (E), and (G) represent pharmacokinetics in the absence of bosentan, while subplots (B), (D), (F), and (H) represent pharmacokinetics in the presence of bosentan.

Figure 5. Simulated total systemic and liver tissue concentrations (A, D, and G), ratios between unbound liver tissue and unbound systemic plasma concentrations (B, E, and H), and induction effect of bosentan (C, F, and I). In subplots (A, D, and G), red and blue curves represent systemic and liver concentrations. In subplots (C, F, and I), red and blue curves represent induction effects in enterocytes and liver. The solid lines and shaded areas represent medina and 95% intervals of the simulations.

Figure 6. Simulated induction effect based on clinical data (green) and in vitro hepatocyte data (red, black, and blue). Red, blue, and black represent simulations based on hepatocyte lots HC7-4, HH1025, and FOS. The solid lines and shaded areas represent medina and 95% intervals of the simulations.

Figure 7. (A) simulated inhibition of BSEP (black), MRP3 (green), and MRP4 (magenta) based on bosentan unbound liver tissue concentration, and (B) simulated inhibition of NTCP (cyan) based on bosentan unbound liver plasma concentration. The solid lines and shaded areas represent medina and 95% intervals of the simulations.

DMD Fast Forward. Published on January 12, 2018 as DOI: 10.1124/dmd.117.078790
This article has not been copyedited and formatted. The final version may differ from this version.

Table 1. Bosentan clinical data included in the PBPK modeling exercise.

Dosed compound(s)	Dosing route	Dosing amount	Reference
Bosentan	Intravenous infusion (5 min)	10, 50, 250, 500, 750 mg	(Weber et al., 1996)
Bosentan	Intravenous infusion (15 min)	250 mg	(Weber et al., 1999b)
Bosentan	Tablet after high fat meal	500 mg	(NDA-21-290, 2001)
Bosentan	Tablet after high fat meal	125 mg	(Dingemanse et al., 2002)
Bosentan	Tablet	500 mg	(Weber et al., 1999c)
Bosentan	Tablet	62.5 mg	(van Giersbergen et al., 2002b)
Bosentan (BID) Tadalafil (QD)	Tablet	125 mg bosentan, 40 mg tadalafil	(Wrishko et al., 2008)
Bosentan (BID) Warfarin (once on day 6)	Tablet	500 mg bosentan 26 mg racemic mixture of warfarin	(Weber et al., 1999a)

Table 2. The list of parameters with fixed values in the described bosentan PBPK model.

Parameter	Unit	Value	Source	Parameter	Unit	Value	Source
pKa		5.2 (acidic)	In-house	k_{on}	$nmol^{-1} \cdot hour^{-1}$	3600	(Alberty and Hammes, 1958)
$logD_{7.4}$		1.3	In-house	$k_{off,plasma}$	$hour^{-1}$	8.18×10^{7}	Supplemental Materials
MW	$g \cdot mol^{-1}$	551.6	In-house	$k_{off,RBC}$	$hour^{-1}$	1.25×10^{7}	Supplemental Materials
$K_{M,liver,uptake}$	nM	4343	SCHH	$k_{off,liver,tissue}$	$hour^{-1}$	4.80×10^{7}	SCHH
$K_{M,liver,metabolism}$	nM	6.9×10^{4}	(Shen et al., 2009)	Binding site in plasma	nM	1.14×10^{6}	Supplemental Materials
$K_{M,enterocyte,metabolism}$	nM	6.9×10^{4}	(Shen et al., 2009)	Binding site in RBC	nM	4.11×10^{4}	Supplemental Materials
Ratio of $k_{enterocyte,metabolism}$ to $k_{liver,metabolism}$		0.0260	Supplemental Materials	Binding site liver tissue	nM	3.67×10^{5}	SCHH
$F_{a,\ 62.5\ mg\ tablet}$		0.973	Supplemental Materials	$CL_{systemic,blood,pass}$	$L \cdot hour^{-1}$	1.12×10^{3}	Supplemental Materials
$F_{a,\ 125\ mg\ tablet}$		1	Supplemental Materials	$CL_{liver,blood,pass}$	$L \cdot hour^{-1}$	72.5	Supplemental Materials
$F_{a,\ 500\ mg\ tablet}$		0.823	Supplemental Materials	$CL_{villi,blood,pass}$	$L \cdot hour^{-1}$	2.43	Supplemental Materials
$F_{a,\ 125\ mg\ high\ fat}$		1	Supplemental Materials	CYP $k_{entercoyte,degradation}$	$hour^{-1}$	0.0300	(Yang et al., 2008)
$F_{a,\ 500\ mg\ high\ fat}$		1	Supplemental Materials	CYP $k_{liver,degradation}$	$hour^{-1}$	0.0250	(Quinney et al., 2010)
Human HCT		0.519	In-house	Induction EC_{50}	nM	1000	Hepatocyte induction assay
$IC_{50,NTCP}$	nM	2.4×10^{4}	(Leslie et al., 2007)	$IC_{50,MRP3}$	nM	4.2×10^{4}	(Morgan et al., 2013)
$IC_{50,BSEP}$	nM	2.3×10^{4}	(Morgan et al., 2013)	$IC_{50,MRP4}$	nM	2.2×10^{4}	(Morgan et al., 2013)

DMD Fast Forward. Published on January 12, 2018 as DOI: 10.1124/dmd.117.078790
This article has not been copyedited and formatted. The final version may differ from this version.

Table 3. Median values and 95% confidence intervals of optimized parameters in the bosentan PBPK model. Values and confidence intervals are estimated by fitting clinical data.

Parameter	Unit	Median	Confidence intervals
ET k_{off}	$hour^{-1}$	1.61×10^{4}	7200, 3.4×10^{4}
ET total concentration	nM	2750	1400, 4900
$CL_{liver,pass}$	$L\cdot hour^{-1}$	23.9	13, 44
$k_{liver,uptake}$	$nmol\cdot hour^{-1}$	4.78×10^{6}	3.8×10^{6}, 6.5×10^{6}
$k_{liver,metabolism}$	$nmol\cdot hour^{-1}$	1.00×10^{6}	8.0×10^{5}, 1.3×10^{6}
$k_{liver,efflux}$	$nmol\cdot hour^{-1}$	6.00×10^{4}	
$K_{m,liver,efflux}$	nM	1.48×10^{6}	
k_a	$hour^{-1}$	0.932	0.81, 1.3
k_a (meal)	$hour^{-1}$	0.759	0.64, 1.1
$f_{u,enterocyte}$		0.964	0.50, 1.0
$CL_{enterocyte,pass}$	$L\cdot hour^{-1}$	2.31×10^{-5}	$< 1.1\times10^{-4}$
$CL_{enterocyte,efflux}$	$L\cdot hour^{-1}$	6.80×10^{-5}	$< 1.1\times10^{-4}$
Clinical induction E_{max}		1.36	1.0, 1.7
Tadalafil F_aF_g with bosentan		0.868	0.70, 1.0
S warfarin F_aF_g with bosentan		1.10	0.99, 1.2
R warfarin F_aF_g with bosentan		1.00	0.83, 1.3

* Median and confidence interval are not provided for the parameters with high uncertainty (i.e., the range of approximated confidence interval is greater than 20 magnitude). The globally optimized values (and upper bound if possible) are provided instead.

DMD Fast Forward. Published on January 12, 2018 as DOI: 10.1124/dmd.117.078790
This article has not been copyedited and formatted. The final version may differ from this version.

Table 4. Median values and 95% confidence intervals of optimized in vitro parameters (E_{max} and EC_{50}) describing CYP induction due to bosentan.

Assay	Hepatocyte lot*	E_{max}	EC_{50} (nM)
CYP2B6 activity	HC7-4	9.62 (8.4 and 11)	1440 (1100 and 1900)
	HH1025	1.40 (1.1 and 1.7)	
	FOS	9.13 (7.9 and 11)	
CYP3A4 activity	HC7-4	11.0 (9.5 and 13)	433 (320 and 590)
	HH1025	1.62 (1.3 and 2.0)	
	FOS	8.26 (7.2 and 9.5)	
CYP2B6 mRNA	HC7-4	11.1 (9.0 and 14)	958 (600 and 1500)
	HH1025	11.2 (9.0 and 14)	
	FOS	3.89 (3.0 and 5.0)	
CYP3A4 mRNA	HC7-4	127 (110 and 150)	1118 (860 and 1500)
	HH1025	72.9 (60 and 89)	
	FOS	29.9 (25 and 36)	

*HC7-4 and FOS are from male donors and HH1025 is from a female donor.

DMD Fast Forward. Published on January 12, 2018 as DOI: 10.1124/dmd.117.078790
This article has not been copyedited and formatted. The final version may differ from this version.

Figure 1.

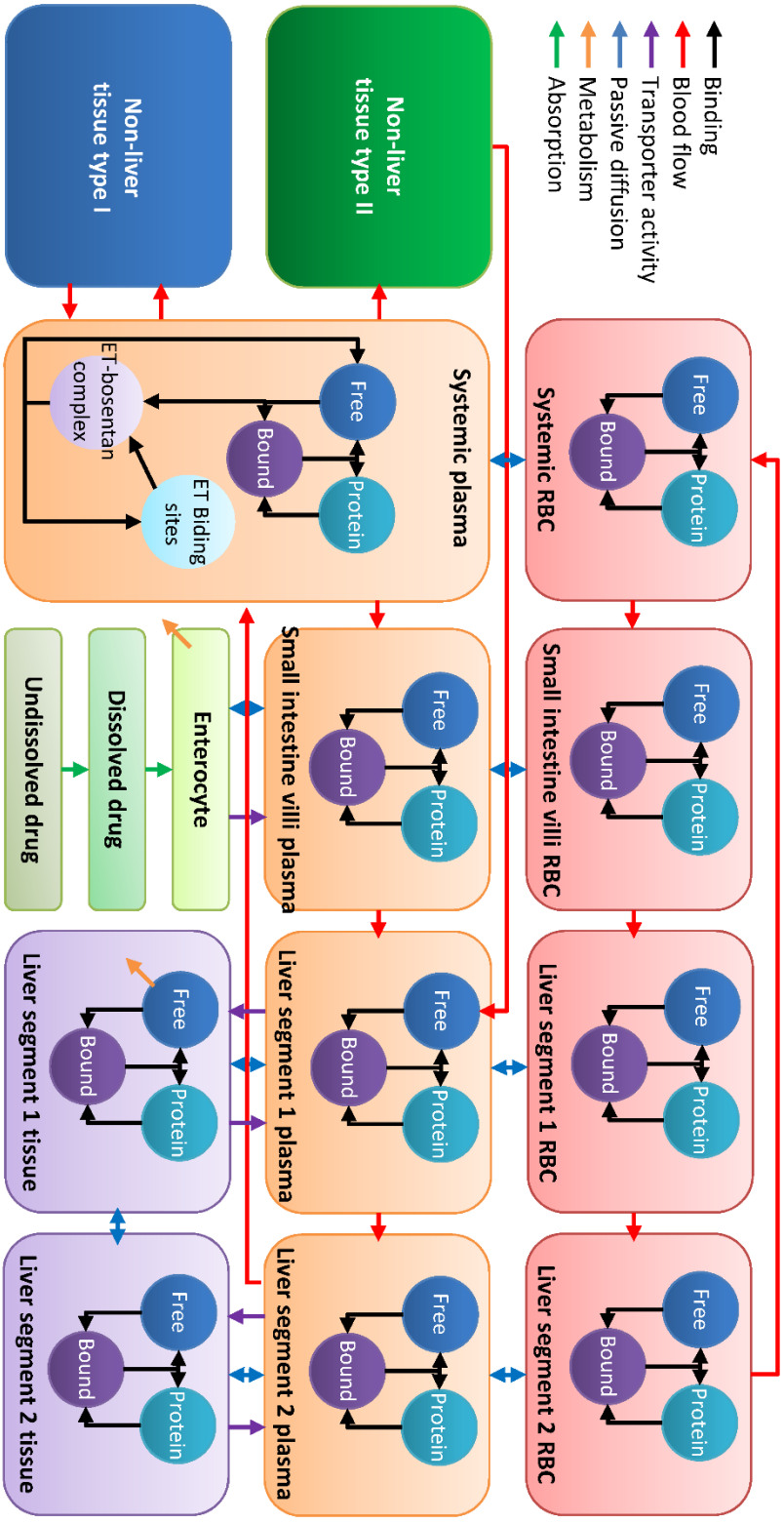

DMD Fast Forward. Published on January 12, 2018 as DOI: 10.1124/dmd.117.078790
This article has not been copyedited and formatted. The final version may differ from this version.

Figure 2.

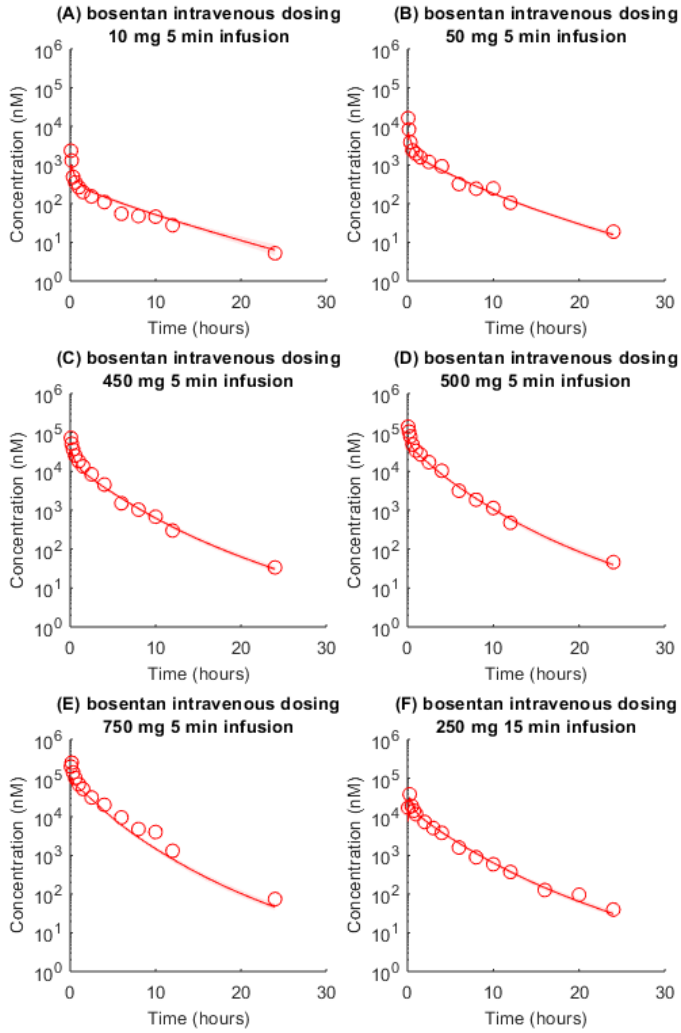

DMD Fast Forward. Published on January 12, 2018 as DOI: 10.1124/dmd.117.078790
This article has not been copyedited and formatted. The final version may differ from this version.

Figure 3.

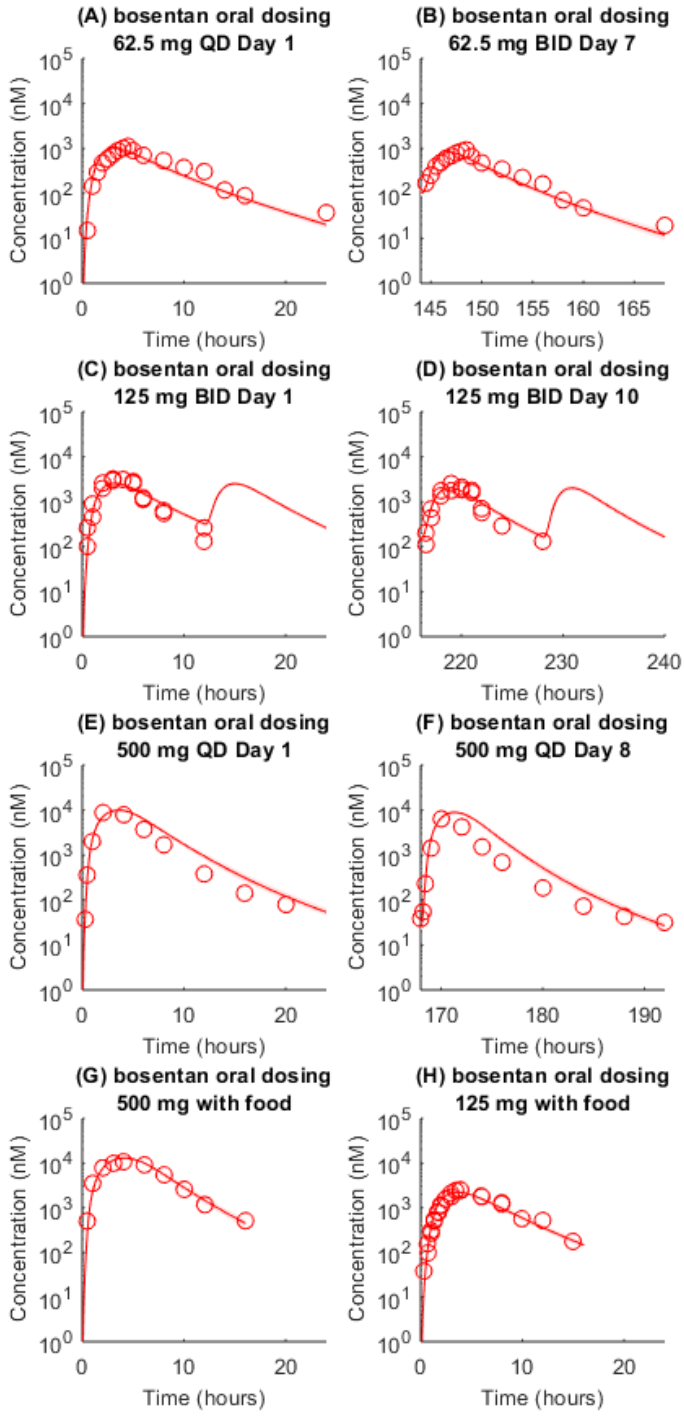

DMD Fast Forward. Published on January 12, 2018 as DOI: 10.1124/dmd.117.078790
This article has not been copyedited and formatted. The final version may differ from this version.

Figure 4.

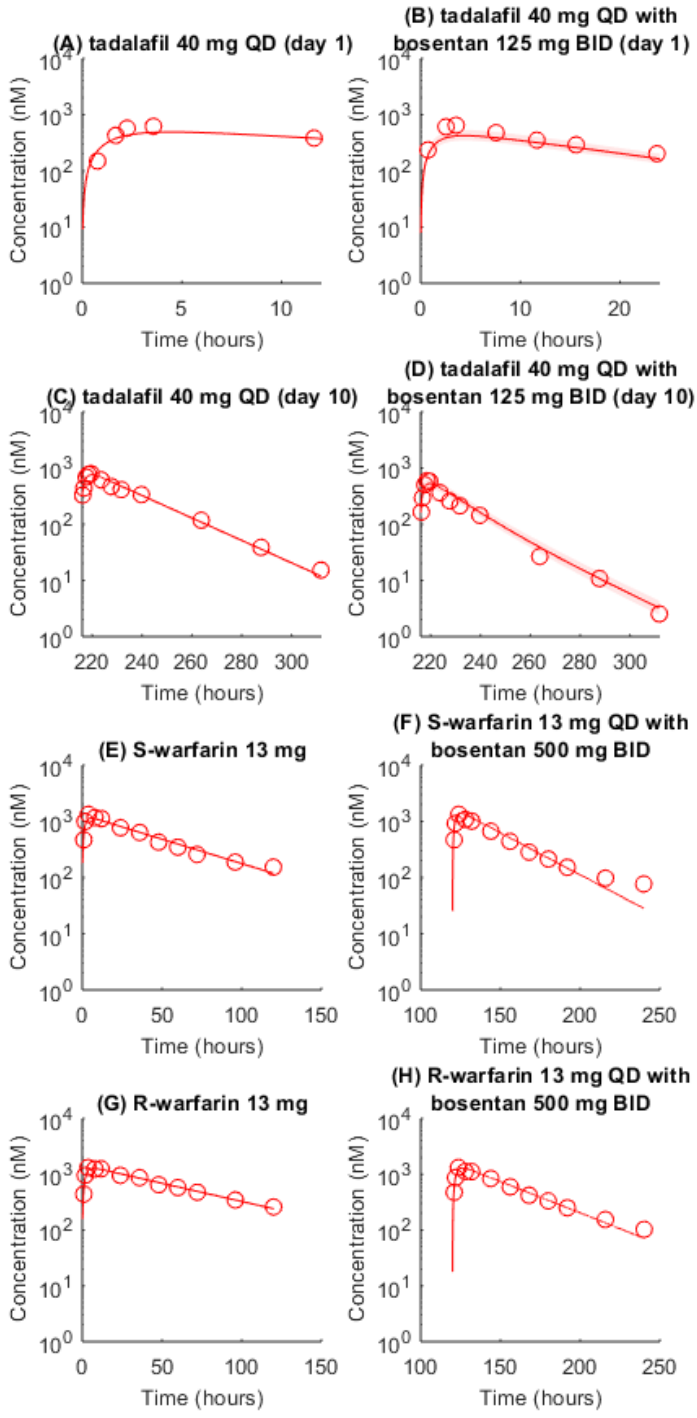

DMD Fast Forward. Published on January 12, 2018 as DOI: 10.1124/dmd.117.078790
This article has not been copyedited and formatted. The final version may differ from this version.

Figure 5.

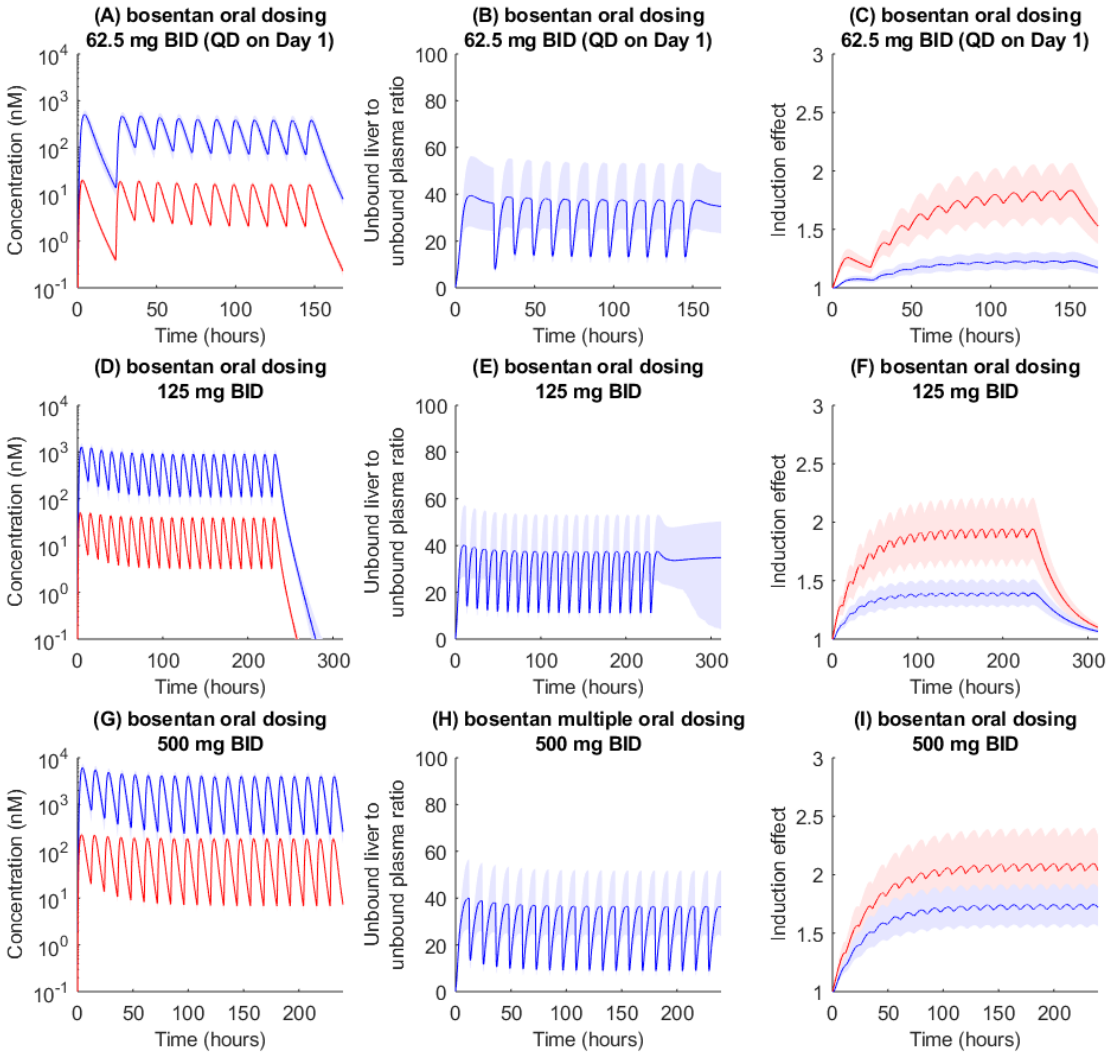

DMD Fast Forward. Published on January 12, 2018 as DOI: 10.1124/dmd.117.078790
This article has not been copyedited and formatted. The final version may differ from this version.

Figure 6.

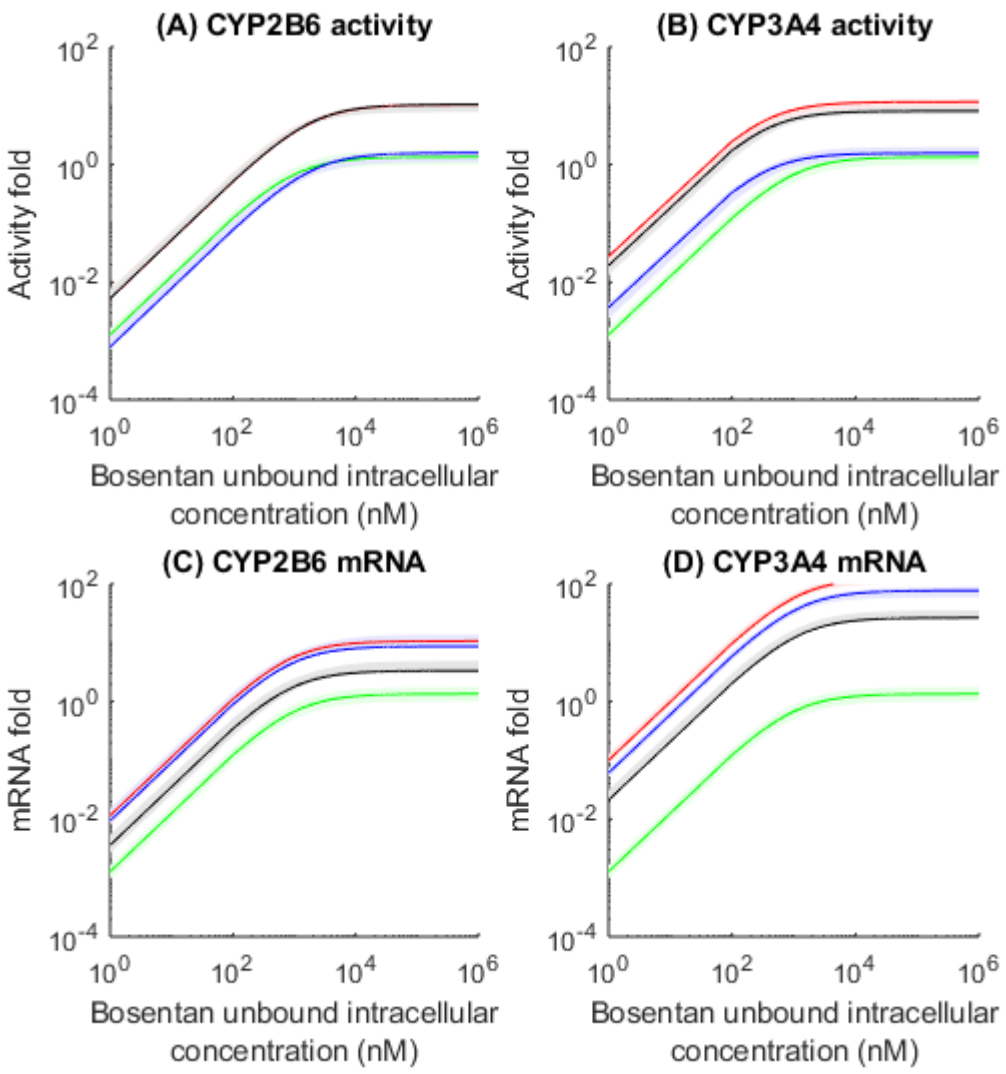

DMD Fast Forward. Published on January 12, 2018 as DOI: 10.1124/dmd.117.078790
This article has not been copyedited and formatted. The final version may differ from this version.

Figure 7.

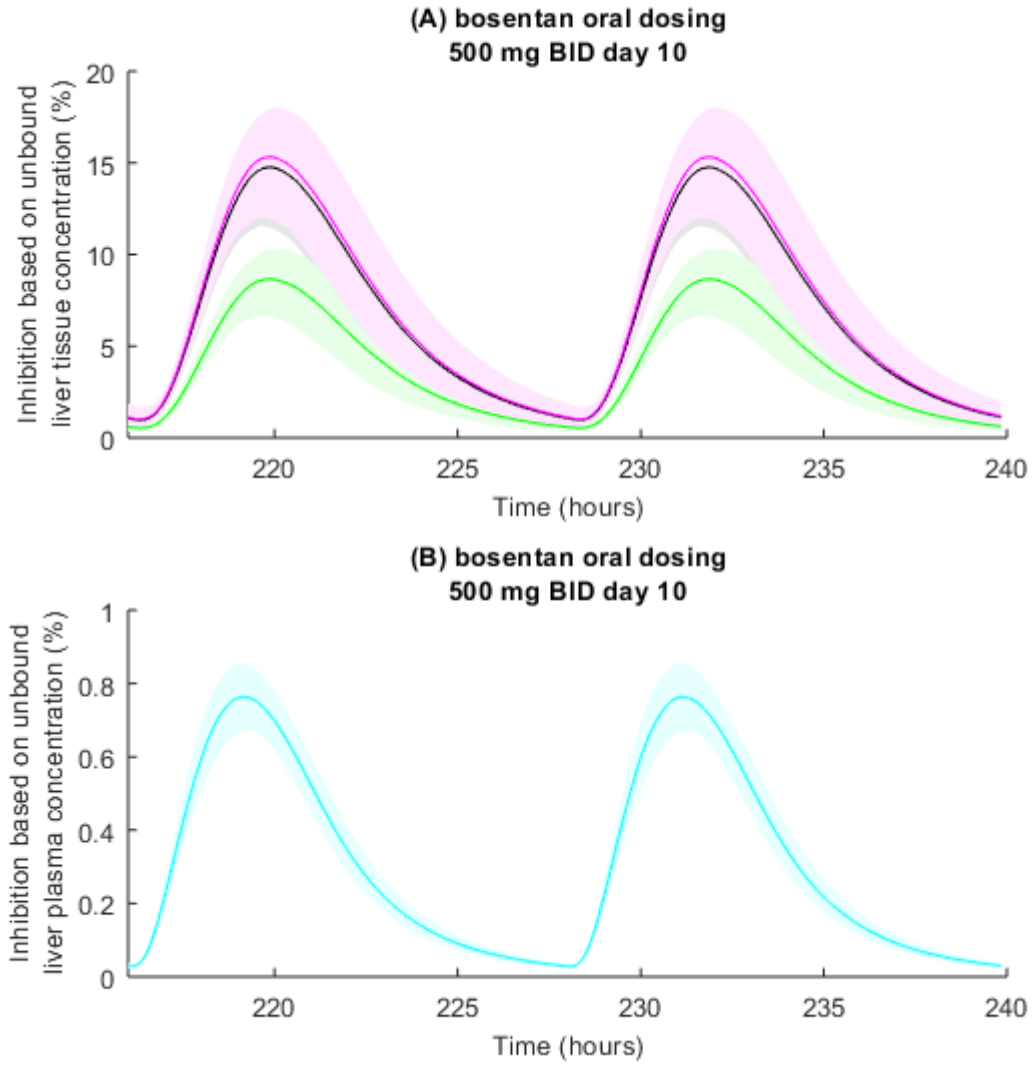

DRUG METABOLISM AND DISPOSITION

Supplemental Materials

A study on pharmacokinetics of bosentan with systems modeling, Part 1: translating systemic plasma concentration to liver exposure in healthy subjects

Rui Li, Mark Niosi, Nathaniel Johnson, David A. Tess, Emi Kimoto, Jian Lin, Xin Yang, Keith A. Riccardi, Sangwoo Ryu, Ayman F. El-Kattan, Tristan S. Maurer, Larry M. Tremaine, and Li Di

A physiologically based pharmacokinetics model for bosentan

Systemic blood model. The arterial blood, venous blood, and lung are lumped together as systemic blood, which is then split into systemic plasma and red blood cells (RBC). Due to potential nonlinear binding kinetics, instead of assuming constant plasma unbound fraction ($f_{u,p}$) or blood to plasma ratio ($R_{B/C}$), we use kinetic model to describe binding in plasma and red blood cells. As such, the binding in the plasma is modeled with mass balances of unbound concentration, bound concentration, and available binding site concentration (Equation 1 to 3)

$$\frac{dC_{unbound}}{dt} = -k_{on} \cdot C_{unbound} \cdot C_{available-site} + k_{off} \cdot C_{bound} \quad (1)$$

$$\frac{dC_{available-site}}{dt} = -k_{on} \cdot C_{unbound} \cdot C_{available-site} + k_{off} \cdot C_{bound} \quad (2)$$

$$\frac{dC_{bound}}{dt} = k_{on} \cdot C_{unbound} \cdot C_{available-site} - k_{off} \cdot C_{bound} \quad (3)$$

Similarly, the distribution in RBC is modeled with mass balances of unbound systemic RBC concentration, bound systemic RBC concentration, and available RBC binding site concentration. We assume that there is a passive permeation between RBC and plasma, hence the kinetics of $R_{B/P}$ depends on the binding in both plasma and RBC.

The target mediated drug disposition (TMDD) has been proposed in a previous study (Volz et al., 2017). Although it is easy to understand that target binding may change the distribution, it is hard to believe that the targets (i.e. endothelin receptors, ET) or their internalization can eliminate the compound without solid biological evidence. As such, in addition to the non-specific binding to the plasma protein for compound in the systemic plasma, specific binding to the ET has been added. Different from binding

to plasma and RBC proteins, the binding parameters to ET are optimized with other parameters by fitting clinical data.

For perfusion-limited tissue compartments, we assume that instantaneous equilibrium between tissue and unbound systemic plasma is limited by blood flow. Except for unbound plasma concentration, the other components in systemic blood do not interact with these tissues directly. On the other hand, all components in the systemic blood are connected with their counterparts in the liver and villi blood, except that we assume target binding in the liver and villi blood is minimal.

The final model (Equation 4 to 8) for systemic plasma incorporates circulation (e.g. the first row of Equation 4), binding to plasma protein (e.g. the second row of Equation 4), diffusion between plasma and RBC (e.g. the third row of Equation 4), and binding to ET (e.g. the forth row of Equation 4), while the model (Equation 9 to 11) for systemic RBC incorporates circulation, binding to RBC protein, and diffusion between plasma and RBC. In the following equations, *HCT* represents hematocrit; *V*, *C*, *Q*, and *T* represent volume, concentration, blood flow, and tissue; *UP*, *BP*, and *ASP* represent unbound plasma, bound plasma, and available binding sites in plasma; *BET* and *ASET* represent bound and unbound ET; *UR*, *BR*, and *ASR* represent unbound RBC, bound RBC, and available binding sites in RBC; $Kp_{,u}$ represents total tissue to unbound plasma concentration ratio; and $CL_{systemic,blood,pass}$ represents passive permeation between unbound systemic RBC and plasma, which is the product of permeability and estimated surface area.

The permeability is calculated as the ratio of SCHH $CL_{HEP,pass}$ (10.8 $uL \cdot min^{-1} \cdot mg^{-1}$) in Part 2 to an assumed hepatocyte surface area (2.30×10^9 $\mu m^2 \cdot mg^{-1}$) of 1 mg protein (i.e. 2.5×10^6 million cells), where we assume a hepatocyte is a sphere with a diameter of 17.1 μm. The volume of a single RBC is assumed to be 90 fL (Turgeon, 2017), while the volume of total RBC in systemic blood is 2.63 L (Table S1). Assuming that RBC is spherical, we can derive the total surface area of RBC in systemic blood as

2.57×10^{14} μm^2. Finally, $CL_{systemic,blood,pass}$ is determined as 1.12×10^{3} L·hour^{-1}. The values of $CL_{liver,blood,pass}$ and $CL_{villi,blood,pass}$ are calculated using the same approach, but with volume of RBC in liver and small intestine villi blood.

$$\begin{aligned}
&V_{systemic,plasma}\cdot\frac{dC_{systemic,UP}}{dt}\\
&=\left[Q_{liver,venous}\cdot C_{liver,UP,5}+\sum_{i=1}^{11}Q_{T,i}\cdot C_{T,i}/Kp_{uT,i}-Q_{total}\cdot C_{systemic,UP}\right]\cdot\left[1-HCT\right]\\
&-\left[k_{on,plasma}\cdot C_{systemic,UP}\cdot C_{systemic,ASP}-k_{off,plasma}\cdot C_{systemic,BP}\right]\cdot V_{systemic,plasma}\\
&-\left[C_{systemic,UP}-C_{systemic,UR}\right]\cdot CL_{systemic,blood,pass}\\
&-\left[k_{on,ET}\cdot C_{systemic,UP}\cdot C_{systemic,ASET}-k_{off,ET}\cdot C_{systemic,BET}\right]\cdot V_{systemic,plasma}
\end{aligned}\tag{4}$$

$$\begin{aligned}
&V_{systemic,plasma}\cdot\frac{dC_{systemic,BP}}{dt}\\
&=\left[Q_{liver,arterial}\cdot C_{liver,BP,5}-Q_{liver,arterial}\cdot C_{systemic,BP}\right]\cdot\left[1-HCT\right]\\
&+\left[k_{on,plasma}\cdot C_{systemic,UP}\cdot C_{systemic,ASP}-k_{off,plasma}\cdot C_{systemic,BP}\right]\cdot V_{systemic,plasma}
\end{aligned}\tag{5}$$

$$\begin{aligned}
&V_{systemic,plasma}\cdot\frac{dC_{systemic,ASP}}{dt}\\
&=\left[Q_{liver,arterial}\cdot C_{liver,ASP,5}-Q_{liver,arterial}\cdot C_{systemic,ASP}\right]\cdot\left[1-HCT\right]\\
&-\left[k_{on,plasma}\cdot C_{systemic,UP}\cdot C_{systemic,ASP}-k_{off,plasma}\cdot C_{systemic,BP}\right]\cdot V_{systemic,plasma}
\end{aligned}\tag{6}$$

$$\frac{dC_{systemic,ASET}}{dt}=k_{on,ET}\cdot C_{systemic,UP}\cdot C_{systemic,ASET}-k_{off,ET}\cdot C_{systemic,BET}\tag{7}$$

$$\frac{dC_{systemic,BET}}{dt}=-k_{on,ET}\cdot C_{systemic,UP}\cdot C_{systemic,ASET}+k_{off,ET}\cdot C_{systemic,BET}\tag{8}$$

$$\begin{aligned}
&V_{systemic,RBC}\cdot\frac{dC_{systemic,UR}}{dt}\\
&=\left[Q_{liver,arterial}\cdot C_{liver,UR,5}-Q_{liver,arterial}\cdot C_{venous,UR}\right]\cdot HCT\\
&-\left[k_{on,RBC}\cdot C_{systemic,UR}\cdot C_{venous,ASR}-k_{off,RBC}\cdot C_{systemic,BR}\right]\cdot V_{systemic,RBC}\\
&+\left[C_{systemic,UP}-C_{systemic,UR}\right]\cdot CL_{systemic,blood,pass}
\end{aligned}\tag{9}$$

$$V_{systemic,RBC} \cdot \frac{dC_{systemic,BR}}{dt} = \left[Q_{liver,arterial} \cdot C_{liver,BR,5} - Q_{liver,arterial} \cdot C_{systemic,BR} \right] \cdot HCT + \left[k_{on,RBC} \cdot C_{systemic,UR} \cdot C_{systemic,ASR} - k_{off,RBC} \cdot C_{systemic,BR} \right] \cdot V_{systemic,RBC} \quad (10)$$

$$V_{systemic,RBC} \cdot \frac{dC_{systemic,ASR}}{dt} = \left[Q_{liver,arterial} \cdot C_{liver,ASR,5} - Q_{liver,arterial} \cdot C_{venous,ASR} \right] \cdot HCT - \left[k_{on,RBC} \cdot C_{systemic,UR} \cdot C_{systemic,ASR} - k_{off,RBC} \cdot C_{systemic,BR} \right] \cdot V_{systemic,RBC} \quad (11)$$

Non-liver tissue distribution model. Perfusion-limited compartments are applied to non-liver tissues. The equilibrium tissue concentration is defined by in silico predicted Kp_u (i.e. total tissue to unbound plasma ratio) values (Rodgers and Rowland, 2006).

$$V_{T,i} \cdot \frac{dC_{T,i}}{dt} = \left[C_{systemic,UP} - C_{T,i} / Kp_{uT,i} \right] \cdot Q_{T,i} \cdot \left[1 - HCT \right] \quad (12)$$

It is unclear if in silico predicted Kp_u value could reasonably represent actual tissue distribution. As such, we employ an empirical scaling factor for the in silico Kp_u, which is optimized with other parameters in fitting clinical data. However, we find that data fitting and liver prediction do not change significantly with and without scaling factor for Kp_u. As such, this scaling factor is removed from the final model.

Liver model. Each liver blood sub-compartment is split into six components (i.e. unbound liver plasma concentration, bound liver plasma concentration, available binding site concentration in liver plasma, unbound liver RBC concentration, bound liver RBC concentration, and available binding site concentration in liver RBC). TMDD is ignored in the liver blood. The hepatic uptake, efflux, and passive diffusion mediate bosentan transport between unbound liver plasma (i.e. *UP*) and unbound liver

tissue (i.e. *UT*). One of five liver blood segments (i.e. the i^{th} segment) is presented here as an example (Equation 13 to 15 for liver plasma, and Equation 16 to 18 for liver RBC). In the following equations, $CL_{liver,blood,pass}$ represents passive permeation between unbound liver RBC and plasma, $CL_{liver,pass}$ represents passive diffusion between unbound liver plasma and unbound liver tissue, $k_{liver,uptake}$ and $k_{liver,efflux}$ represent active uptake and efflux rates, and $K_{M,liver,uptake}$ and $K_{M,liver,efflux}$ represent Michaelis-Menten constant.

$$
\begin{aligned}
& V_{liver,plasma,i}\frac{dC_{liver,UP,i}}{dt} \\
&= \left[C_{liver,UP,i\text{-}1} - C_{liver,UP,i}\right]\cdot Q_{liver,venous}\cdot\left[1-HCT\right] \\
&-\left[k_{on,plasma}\cdot C_{liver,UP,i}\cdot C_{liver,ASP,i} - k_{off,plasma}\cdot C_{liver,BP,i}\right]\cdot V_{liver,plasma,i} \\
&-\left[C_{liver,UP,i} - C_{liver,UR,i}\right]\cdot CL_{liver,blood,pass} \\
&-\left[C_{liver,UP,i} - C_{liver,UT,i}\right]\cdot CL_{liver,pass}/5 \\
&-C_{liver,UP,i}/\left[C_{liver,UP,i} + K_{M,liver,uptake}\right]\cdot k_{liver,uptake}/5 \\
&+C_{liver,UT,i}/\left[C_{liver,UT,i} + K_{M,liver,efflux}\right]\cdot k_{liver,efflux}/5
\end{aligned}
\tag{13}
$$

$$
\begin{aligned}
& V_{liver,plasma,i}\cdot\frac{dC_{liver,ASP,i}}{dt} \\
&= \left[C_{liver,ASP,i-1} - C_{liver,ASP,i}\right]\cdot\left[Q_{liver,arterial} + Q_{villi}\right]\cdot\left[1-HCT\right] \\
&-\left[k_{on,plasma}\cdot C_{liver,UP,i}\cdot C_{liver,ASP,i} - k_{off,plasma}\cdot C_{liver,BP,i}\right]\cdot V_{liver,plasma,i}
\end{aligned}
\tag{14}
$$

$$
\begin{aligned}
& V_{liver,plasma,i}\cdot\frac{dC_{liver,BP,i}}{dt} \\
&= \left[C_{liver,BP,i-1} - C_{liver,BP,i}\right]\cdot\left[Q_{liver,arterial} + Q_{villi}\right]\cdot\left[1-HCT\right] \\
&+\left[k_{on,plasma}\cdot C_{liver,UP,i}\cdot C_{liver,PP,i} - k_{off,plasma}\cdot C_{liver,BP,i}\right]\cdot V_{liver,plasma,i}
\end{aligned}
\tag{15}
$$

$$
\begin{aligned}
&V_{liver,RBC,i} \cdot \frac{dC_{liver,UR,i}}{dt} \\
&= \left[C_{liver,UR,i-1} - C_{liver,UR,i} \right] \cdot \left[Q_{liver,arterial} + Q_{villi} \right] \cdot HCT \\
&- \left[k_{on,RBC} \cdot C_{liver,UR,i} \cdot C_{liver,ASR,i} - \cdot k_{off,RBC} \cdot C_{liver,BR,i} \right] \cdot V_{liver,RBC,i} \\
&+ \left(C_{liver,UP,i} - C_{liver,UR,i} \right) \cdot CL_{liver,blood,pass}
\end{aligned} \tag{16}
$$

$$
\begin{aligned}
&V_{liver,RBC,i} \cdot \frac{dC_{liver,ASR,i}}{dt} \\
&= \left[C_{liver,ASR,i-1} - C_{liver,ASR,i} \right] \cdot \left[Q_{liver,arterial} + Q_{villi} \right] \cdot HCT \\
&- \left[k_{on,RBC} \cdot C_{liver,UR,i} \cdot C_{liver,ASR,i} - k_{off,RBC} \cdot C_{liver,BR,i} \right] \cdot V_{liver,RBC,i}
\end{aligned} \tag{17}
$$

$$
\begin{aligned}
&V_{liver,RBC,i} \cdot \frac{dC_{liver,BR,i}}{dt} \\
&= \left[C_{liver,BR,i-1} - C_{liver,BR,i} \right] \cdot \left[Q_{liver,arterial} + Q_{villi} \right] \cdot HCT \\
&+ \left[k_{on,RBC} \cdot C_{liver,UR,i} \cdot C_{liver,ASR,i} - k_{off,RBC} \cdot C_{liver,BR,i} \right] \cdot V_{liver,RBC,i}
\end{aligned} \tag{18}
$$

Within the liver tissue, the binding kinetics is explicitly modeled with k_{on} and k_{off} rates. Metabolism is modeled using metabolic rate and Machiens-Menton constant (i.e. $k_{liver,metabolism}$ and $K_{M,liver,metabolism}$). The biliary excretion is assumed to be zero based on the in vitro data (SCHH, Part 2 of this study published in a separated article) and in vivo observation that minimal compound is excreted into feces following intravenous dosing (Weber et al., 1999b). One of five liver tissue segments (i.e. the i^{th} segment) is presented here as an example (Equation 19 to 21). In these equations, *UT*, *BT*, and *AST* represent unbound tissue, bound tissue, and available binding sites in liver tissue. In Equation 19, the first row represents passive diffusion among tissue compartments, the second to the forth rows represent transport between unbound liver plasma and tissue, the fifth row represents metabolism, and the last row represents the binding kinetics. $E_{liver,induction,i}$ represents the induction effect in each segment which is explained below (Equation 32).

$$
\begin{aligned}
&V_{liver,tissue,i}\frac{dC_{liver,UT,i}}{dt}\\
&=\left[C_{liver,UT,i-1}+C_{liver,UT,i+1}-2\cdot C_{liver,UT,i}\right]\cdot CL_{liver,pass}/\left[5\times 2\right]\\
&+\left[C_{liver,UP,i}-C_{liver,UT,i}\right]\cdot CL_{liver,pass}/5\\
&+C_{liver,UP,i}/\left[C_{liver,UP,i}+K_{M,liver,uptake}\right]\cdot k_{liver,uptake}/5\\
&-C_{liver,UT,i}/\left[C_{liver,UT,i}+K_{M,liver,efflux}\right]\cdot k_{liver,efflux}/5\\
&-C_{liver,UT,i}/\left[C_{liver,UT,i}+K_{M,liver,metabolism}\right]\cdot k_{liver,metabolism}\cdot E_{liver,induction,i}/5\\
&+\left[k_{off,liver,tissue}\cdot C_{liver,BT,i}-k_{on,liver,tissue}\cdot C_{liver,UT,i}\cdot C_{liver,AST,i}\right]\cdot V_{liver,tissue,i}
\end{aligned}
\tag{19}
$$

$$
\frac{dC_{liver,AST,i}}{dt}=-k_{on,tissue}\cdot C_{liver,UT,i}\cdot C_{liver,AST,i}+k_{off,tissue}\cdot C_{liver,BT,i} \tag{20}
$$

$$
\frac{dC_{liver,BT,i}}{dt}=k_{on,tissue}\cdot C_{liver,UT,i}\cdot C_{liver,AST,i}-k_{off,tissue}\cdot C_{liver,BT,i} \tag{21}
$$

Absorption model. The oral absorption is modeled with a semi-mechanistic model. The orally administrated drug enters the model from the undissolved compartment, where it is transferred to the dissolved compartment with a first order rate constant (k_a) and scaled by fraction absorbed (F_a). The dissolved drug is transferred into the enterocyte also with the first order rate k_a. Since both k_a are parameter estimated by fitting clinical data, and are not uniquely distinguishable, we assume two k_a share the same value. We assume that 100% dissolved drug enters enterocyte in the model, because additional fraction parameter in this step would have the same impact on simulations as F_a. Once the drug enters enterocyte, it can be either metabolized, or transferred into villi blood by passive diffusion or active efflux. An enterocyte intracellular unbound fraction is applied and estimated by fitting clinical data with fitted other parameters. We assume that there is no active uptake from blood into enterocyte. Similar to blood in the systemic circulation and liver, villi blood is also split into six compartments to model binding in plasma and RBC (Equation 25 to 30).

$$\frac{dA_{undissolved}}{dt} = -k_a \cdot A_{undissolved} \tag{22}$$

$$\frac{dA_{dissolved}}{dt} = k_a \cdot A_{undissolved} \cdot F_a - k_a \cdot A_{dissolved} \tag{23}$$

$$\begin{aligned} & V_{enterocyte} \cdot \frac{dC_{enterocyte}}{dt} \\ & = k_a \cdot A_{dissolved} \\ & - C_{enterocyte} \cdot f_{u,enterocyte} \Big/ \left[C_{enterocyte} \cdot f_{u,enterocyte} + K_{M,gut,metabolism} \right] \cdot k_{enterocyte,metabolism} \cdot E_{eneterocyte,induction} \\ & - C_{enterocyte} \cdot f_{u,enterocyte} \cdot CL_{enterocyte,efflux} \\ & - \left[C_{enterocyte} \cdot f_{u,enterocyte} - C_{villi,UP} \right] \cdot CL_{enterocyte,pass} \end{aligned} \tag{24}$$

$$\begin{aligned} & V_{villi,plasam} \frac{dC_{villi,UP}}{dt} \\ & = \left[C_{systemic,UP} - C_{villi,UP} \right] \cdot Q_{villi} \cdot \left[1 - HCT \right] \\ & + \left[C_{enterocyte} \cdot f_{u,enterocyte} - C_{villi,UP} \right] \cdot CL_{enterocyte,pass} \\ & + C_{enterocyte} \cdot f_{u,enterocyte} \cdot CL_{enterocyte,efflux} \\ & - \left[C_{villi,UP} - C_{villi,UR} \right] \cdot CL_{villi,blood,pass} \end{aligned} \tag{25}$$

$$\begin{aligned} & V_{villi,plasma} \cdot \frac{dC_{villi,ASP}}{dt} \\ & = \left[C_{systemic,ASP} - C_{villi,ASP} \right] \cdot Q_{villi} \cdot \left[1 - HCT \right] \\ & - \left[k_{on,plasma} \cdot C_{villi,UP} \cdot C_{villi,ASP} - k_{off,plasma} \cdot C_{villi,BP} \right] \cdot V_{villi,plasma} \end{aligned} \tag{26}$$

$$\begin{aligned} & V_{villi,plasma} \cdot \frac{dC_{villi,BP}}{dt} \\ & = \left[C_{systemic,BP} - C_{villi,BP} \right] \cdot Q_{villi} \cdot \left[1 - HCT \right] \\ & + \left[k_{on,plasma} \cdot C_{villi,UP} \cdot C_{villi,ASP} - k_{off,plasma} \cdot C_{villi,BP} \right] \cdot V_{villi,plasma} \end{aligned} \tag{27}$$

$$
\begin{aligned}
&V_{villi,RBC} \cdot \frac{dC_{villi,UR}}{dt} \\
&= \left[C_{systemic,UR} - C_{villi,UR} \right] \cdot Q_{villi} \cdot HCT \\
&- \left[k_{on,RBC} \cdot C_{villi,UR} \cdot C_{villi,ASR} - k_{off,RBC} \cdot C_{villi,BR} \right] \cdot V_{villi,RBC} \\
&+ \left[C_{villi,UP} - C_{villi,UR} \right] \cdot CL_{villi,blood,pass}
\end{aligned} \tag{28}
$$

$$
\begin{aligned}
&V_{villi,RBC} \cdot \frac{dC_{villi,ASR}}{dt} \\
&= \left[C_{systemic,ASR} - C_{villi,ASR} \right] \cdot Q_{villi} \cdot HCT \\
&- \left[k_{on,RBC} \cdot C_{villi,UR} \cdot C_{villi,ASR} - k_{off,RBC} \cdot C_{villi,BR} \right] \cdot V_{villi,RBC}
\end{aligned} \tag{29}
$$

$$
\begin{aligned}
&V_{villi,RBC} \cdot \frac{dC_{villi,BR}}{dt} \\
&= \left[C_{systemic,BR} - C_{villi,BR} \right] \cdot Q_{villi} \cdot HCT \\
&+ \left[k_{on,RBC} \cdot C_{villi,UR} \cdot C_{villi,ASR} - k_{off,RBC} \cdot C_{villi,BR} \right] \cdot V_{villi,RBC}
\end{aligned} \tag{30}
$$

The total volume of all enterocytes is assumed to the same as the volume of the small intestine (i.e. 0.30 L (Shah and Betts, 2012)). The free fraction in the enterocyte is a parameter estimated by fitting clinical observation; hence it would adjust the intracellular free concentration if enterocyte volume was mis-specified. According to a previous study with oral dosed suspension, 30.2% of unchanged bosentan is excreted into feces (Weber et al., 1999b). As such, F_a can be approximated as 0.698 for suspension. Assuming different formulation of bosentan share the same hepatic extraction ratio (F_h) and fraction escaping gut metabolism (F_g), F_a will be proportional to plasma exposure after oral dosing. From $AUC_{0-\infty}$ of 24290 and 9022 ng·mL^{-1}·hour for 500 mg oral suspension and 125 mg tablet in tadalafil DDI study (Weber et al., 1999b; Wrishko et al., 2008), we can derive bosentan F_a in tadalafil DDI study as one. Similarly, F_a is estimated to be one for 125 mg and 500 mg tablets with high fat meal based on reported $AUC_{0-\infty}$ of 8791 and 43199 ng·mL^{-1}·hour (NDA-21-290, 2001; Dingemanse et al., 2002); 0.973 for 62.5 mg tablet based on AUC of 4234 ng·mL^{-1}·hour in ketoconazole DDI study (van

Giersbergen et al., 2002); 0.786, 0.991, and 0.909 for 100, 200, and 500 mg tablets based on $AUC_{0-\infty}$ of 5469, 13800, and 31640 ng·mL^{-1}·hour in a multiple ascending oral dose study (Weber et al., 1999c); and 0.736 for 500 mg tablets based on reported $AUC_{0-\infty}$ of 25600 ng·mL^{-1}·hour in a multiple oral dose study (Weber et al., 1999c). In the warfarin DDI study (Weber et al., 1999a), since bosentan pharmacokinetics is not reported, we have to assume that F_a for 500 mg tablet here is the average of 0.909 and 0.736 (i.e. 0.823).

The metabolic rate in the enterocyte ($k_{enterocyte,metabolism}$) is scaled from rate in the liver ($k_{liver,metabolism}$). Based on a human hepatocyte study performed in this study, CYP3A and 2C9 represent 70% and 10% of total hepatic metabolism. As such, from the value of $k_{liver,metabolism}$, the metabolic rates for hepatic CYP3A and 2C9 can be calculated as $k_{liver,metabolism} \times 0.7$ and $k_{liver,metabolism} \times 0.1$. Using human liver microsome assays, the abundances of CYP3A and 2C9 in the human liver have been reported to be 70.8 and 130.3 pmol·mg^{-1} (the averaged values from (Groer et al., 2014; Nakamura et al., 2016)). Assuming liver weight is 1.69×10^3 g (Shah and Betts, 2012) and microsomal protein (mg) per gram of liver (MPPGL) of 45, the specific metabolic rate for CYP3A and 2C9 are $k_{liver,metabolism} \times 0.7 / (70.8 \times 45 \times 1.69\times10^3)$ and $k_{liver,metabolism} \times 0.1 / (130.3 \times 45 \times 1.69\times10^3)$. Using human intestinal microsome assays, the abundances of CYP3A and 2C9 in the human small intestine have been reported to be 22.5 and 3.61 pmol·mg^{-1} (the averaged values from (Groer et al., 2014; Nakamura et al., 2016)). Assuming small intestine weight is 3.74×10^2 g (Shah and Betts, 2012) and microsomal protein (mg) per gram of intestine (MPPGI) of 20.6, the metabolic rate for CYP3A and 2C9 are $k_{liver,metabolism} \times 0.7 / (70.8 \times 45 \times 1.69 \times 10^3) \times (22.5 \times 20.6 \times 3.74\times10^2)$ and $k_{liver,metabolism} \times 0.1 / (130.3 \times 45 \times 1.69 \times 10^3) \times (3.61 \times 20.6 \times 3.74\times10^2)$. As a result, assuming that $k_{enterocyte,metabolism}$ is assumed to be the sum of CYP3A and 2C9 rates in the small intestine, the ratio of $k_{enterocyte,metabolism}$ to $k_{liver,metabolism}$ is 0.0260. Based on estimate $k_{liver,metabolism}$ value of 2.12×10^6 nmol·hour^{-1}, the value of $k_{enterocyte,metabolism}$ is 5.52×10^4 nmol·hour^{-1}.

Induction model. A turnover model is developed to describe in vivo CYP induction effect ($E_{induction}$), where $k_{synthesis}$ and $k_{degradatin}$ represent CYP synthesis and degradation rates. $k_{degradatin}$ is calculated as natural logarithm of 2 divided by CYP half-life. Multiple half-life values for CYP has been published, we pick the approach relying on the inactivation of CYP in clinical study. Induction is a relatively slow process, as such, the estimated half-life could be confounded by the residual effect of inducer even though inducer has been cleared from the body. On the other hand, inactivation is relatively fast. As far as the half-life of inactivator is short enough, the estimated half-life is minimally confounded. $k_{synthesis}$ is set to the same as $k_{degradatin}$ in order to keep base level of $E_{induction}$ at one in the absence of inducer. Five liver tissue segments and enterocyte have independent $E_{induction}$ calculation depending on unbound drug concentration in those tissues. The metabolic rates in liver tissue and gut are scaled by $E_{induction}$. In the absence of inducer, the $E_{induction}$ is a constant of one without affecting metabolism

$$\begin{aligned}&\frac{dE_{liver,induction,i}}{dt}\\&= k_{liver,synthesis}\cdot E_{max,liver,induction}\cdot\frac{C_{liver,UT,i}}{C_{liver,UT,i}+EC_{50,liver,induction}}\\&+k_{liver,synthesis}-k_{liver,degradation}\cdot E_{liver,induction,i}\end{aligned} \tag{31}$$

$$\begin{aligned}&\frac{dE_{enterocyte,induction}}{dt}\\&= k_{enterocyte,synthesis}\cdot E_{max,enterocyte,induction}\cdot\frac{C_{enterocyte}\cdot f_{u,enterocyte}}{C_{enterocyte}\cdot f_{u,enterocyte}+EC_{50,enterocyte,induction}}\\&+k_{enterocyte,synthesis}-k_{enterocyte,degradation}\cdot E_{enterocyte,induction}\end{aligned} \tag{32}$$

Victim model. A reduced PBPK model is developed for the drugs co-dosed with bosentan. Only systemic plasma, well-stirred liver, and empirical absorption compartments are included in this model

(Equation 34 to 36). In the following equations, $V_{central}$, Kp_{liver}, $R_{B/P}$, $f_{u,p}$, and CL_{liver} represent volume of central compartment, liver tissue to plasma partition coefficient, blood to plasma ratio, unbound fraction in plasma, and intrinsic hepatic clearance mediated by metabolism. $E_{liver,induction,i}$ values from five liver segments in bosentan model are averaged and used to scale CL_{liver} of victim compounds. Unfortunately, for victim drugs, there are not enough data to separate gut metabolism from absorption, hence induction is modeled implicitly as different F_aF_g values in the presence and absence of bosentan.

$$V_{central,victim} \cdot \frac{dC_{system,victim}}{dt} = \left[C_{liver,victim} / Kp_{liver,victim} \cdot R_{B/P,victim} - C_{system,victim} \right] \cdot Q_{liver,venous} \quad (33)$$

$$\begin{aligned} V_{liver,tissue} \cdot \frac{dC_{liver,victim}}{dt} &= \left[C_{system,victim} - C_{liver,victim} / Kp_{liver,victim} \cdot R_{B/P,victim} \right] \cdot Q_{liver,venous} \\ &- C_{liver,victim} / Kp_{liver,victim} \cdot f_{u,p,victim} \cdot CL_{liver,victim} \cdot E_{liver,induction} \\ &+ k_{a,victim} \cdot A_{absorption,victim} \cdot F_aF_{g,victim} \end{aligned} \quad (34)$$

$$\frac{dA_{absorption,victim}}{dt} = -k_{a,victim} \cdot A_{absorption,victim} \quad (35)$$

The physiological parameters in victim models have the same values as those in bosentan model. Kp_{liver} is calculated with in silico method as mentioned above. $R_{B/P}$ and $f_{u,p}$ are fixed at in house determined values. $V_{central}$, CL_{liver} and k_a are estimated by fitting clinical data of victim drugs in the absence of bosentan. S- and R-warfarin are fitted independently assuming racemic dosing include equal amount of equal amounts of left- and right-handed enantiomers, however to simplify the problem, we ignored potential inter-conversion between the two compounds after dosing. F_aF_g in the absence of bosentan is arbitrarily fixed at one as because the value of this parameter will not affect our interpretation of data.

On the other hand, F_aF_g values in the presence of bosentan are estimated by fitting clinical data, simultaneously with parameters of bosentan.

BSEP, MRP, NTCP inhibition. Simple competitive inhibition on four transporters is calculated independently based on simulated unbound bosentan concentrations. Because it is unclear if inhibition is driven by intracellular or extracellular bosentan, we have tried two scenarios with either predicted unbound liver tissue or liver plasma (not systemic plasma) concentration. Because the impact of these transporters on bosentan disposition is unclear, hence their inhibition is included in the PBPK model assuming minimal impact on bosentan exposure.

Parameter optimization and predicting liver exposure. Parameter estimation is performed with a previously developed numerical global optimizer (i.e. differential evolution, http://www1.icsi.berkeley.edu/~storn/code.html). MCMC (Markov chain Monte Carlo) toolbox for MATLAB (http://helios.fmi.fi/~lainema/mcmc/) is used to quantify the uncertainty. Starting from the globally optimized parameter values, the toolbox can provide ranges of parameter values that are able to reasonably describe the data. We randomly sample 1000 set of parameter values from all values (8×10^5 sets) identified from MCMC that can adequately describe plasma data. 1000 simulations using sampled parameter values are generated, such that uncertainty in parameter estimation is reflected in simulations.

A mechanistic model to analyze in vitro plasma free fraction and blood to plasma ratio data

The model includes concentrations of unbound compound ($C_{plasma,U}$), bound compound ($C_{plasma,B}$), and protein available for binding ($C_{plasma,P}$) in the plasma, as well as unbound compound ($C_{RBC,U}$), bound compound ($C_{RBC,B}$), and protein available for binding ($C_{RBC,P}$) in the red blood cells (RBC). Assuming the binding between compound and protein is non-specific in both plasma and blood, the mass balances are given as below.

$$\frac{dC_{plasma,U}}{dt} = -k_{on,plasma} \cdot C_{plasma,U} \cdot C_{plasma,P} + k_{off,plasma} \cdot C_{plasma,B} + \frac{CL_{blood,pass}}{V_{plasma}} \cdot \left[C_{RBC,U} - C_{plasma,U} \right] \tag{36}$$

$$\frac{dC_{plasma,B}}{dt} = k_{on,plasma} \cdot C_{plasma,U} \cdot C_{plasma,P} - k_{off,plasma} \cdot C_{plasma,B} \tag{37}$$

$$\frac{dC_{plasma,P}}{dt} = -k_{on,plasma} \cdot C_{plasma,U} \cdot C_{plasma,P} + k_{off,plasma} \cdot C_{plasma,B} \tag{38}$$

$$\frac{dC_{RBC,U}}{dt} = -k_{on,RBC} \cdot C_{RBC,U} \cdot C_{RBC,P} + k_{off,RBC} \cdot C_{RBC,B} - \frac{CL_{blood,pass}}{V_{plasma}} \cdot \left[C_{RBC,U} - C_{plasma,U} \right] \tag{39}$$

$$\frac{dC_{RBC,B}}{dt} = k_{on,RBC} \cdot C_{RBC,U} \cdot C_{RBC,P} - k_{off,RBC} \cdot C_{RBC,B} \tag{40}$$

$$\frac{dC_{RBC,P}}{dt} = -k_{on,RBC} \cdot C_{RBC,U} \cdot C_{RBC,P} + k_{off,RBC} \cdot C_{RBC,B} \tag{41}$$

$$f_{u,p} = \frac{C_{plasma,U}}{C_{plasma,U} + C_{plasma,B}} \tag{42}$$

$$
\begin{aligned}
R_{B/P} &= \frac{C_{blood}}{C_{plasma}} \\
&= \frac{C_{RBC} \cdot V_{RBC} + C_{plasma} \cdot V_{plasma}}{V_{blood} \cdot C_{plasma}} \\
&= \frac{C_{RBC,U} + C_{RBC,B}}{C_{plasma,U} + C_{plasma,B}} \cdot HCT + \left[1 - HCT\right]
\end{aligned}
\tag{43}
$$

HCT (i.e. hematocrit, the volume percentage of red blood cells in blood) is determined in the experiments. Given the data are not enough to estimate values for all binding kinetic parameters, association rates ($k_{on,plasma}$ and $k_{on,RBC}$) are fixed at 10^9 $mol^{-1} \cdot sec^{-1}$ assuming the reaction is limited by diffusion (Alberty and Hammes, 1958). The dissociation rates ($k_{off,plasma}$ and $k_{off,RBC}$), initial conditions for $C_{plasma,P}$ and $C_{plasma,P}$ are estimated by fitting observed $R_{B/P}$ and $f_{u,p}$ at different compound concentrations.

The data used for parameter estimation are presented in Figure S1. The estimated k_{off} rates and the concentration of binding sites are given in the Table 2.

In vitro induction assay and modeling

The induction assay was performed as following. Media free fraction ($f_{u,inc}$ 0.38) was measured to account for the binding due to bovine serum albumin in the media. We assume that intracellular concentration of bosentan in the induction assay is the same as that in the sandwich cultured human hepatocyte (SCHH) assay. As such, the intracellular concentration is simulated with model structure and parameter values published in an SCHH study (presented in Part 2 of this study, which is published in a separated article). To validate this assumption, we measure and simulate the intracellular concentration at 24 hours after initiating the induction assay. The difference between measured concentration and simulation is less than 2 fold, within the variability of the assay.

The turnover model described above for in vivo induction is used to estimate E_{max} and EC_{50} for CYP induction assay, except that the effect is driven by the unbound intracellular concentration simulated with SCHH model. Data from different hepatocyte lots are simultaneously model with shared EC_{50} but specific E_{max} for each lot.

In vitro cytochrome P450 (CYP) reaction phenotyping assay

The assay is performed as described previously using suspension human hepatocyte and selective inhibitors (Yang et al., 2016). The selective CYP 2C9 inactivator (i.e. tienilic acid) and 3A inactivator (i.e. troleandomycin) lead to 10% and 70% inhibition, respectively.

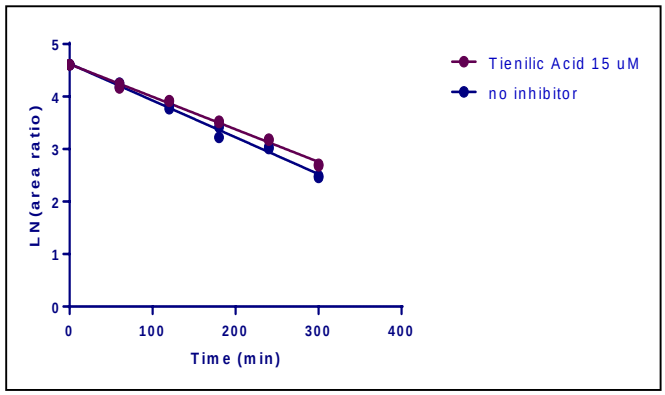

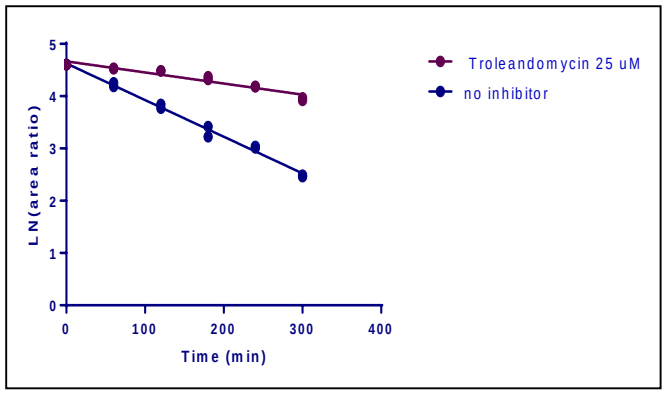

Table S1. Values for physiological parameters.

Tissue	Blood flow ($L \cdot hour^{-1} \cdot kg^{-1}$)	Volume ($L \cdot kg^{-1}$)
Adipose	0.222	0.143
Bone	0.216	0.124
Brain	0.6	0.0207
Gut [2]	0.558	0.0258
Villi blood [3]	0.256	0.000157
Heart	0.128	0.0038
Kidney	0.942	0.0044
Liver blood (arterial) [4]	0.266	0.00468
Liver tissue	-	0.0241
Muscle	0.642	0.429
Pancreas	0.114	0.0012
Skin	0.258	0.111
Spleen	0.066	0.0027
Systemic blood [5]	-	0.0723
Remaining [6]	0.0024	0.0288
Total [7]	4.26	1

1. All the values (except for those noted below) are calculated based on a previous publication (Peters, 2012).
2. The gut volume is calculated as the sum of the reported values for gut and stomach. Its blood flow is the sum of the reported values for gut and stomach minus villi blood flow.
3. Human villi blood flow is reported by (Yang et al., 2007). Shah and Betts reported the small intestine blood volume as 0.000157 $L \cdot kg^{-1}$ (Shah and Betts, 2012). We assume that this volume is the same as villi blood volume.
4. The arterial liver blood flows are calculated by removing gut, pancreas, and spleen values from reported liver values. Shah and Betts report the liver blood volumes (Shah and Betts, 2012).
5. The systemic blood volumes are the sums of the reported venous and arterial volumes minus liver blood volumes. HCT value (i.e. 0.52) is determined experimentally in house to separate blood volumes into RBC and plasma volumes.

6. The values for the rest of body are calculated to keep the mass balance.
7. The total blood flows (i.e. cardiac outputs) are the reported lung blood flows for monkey and rat, and the sum of all report blood flows excluding lung for human.

Table S2. The list of parameters with fixed values in victim model.

Parameter	Unit	Value	Source	Parameter	Unit	Value	Source
			Tadalafil				
k_a	$hour^{-1}$	0.629	See comment below	$R_{B/P}$		1.39	In house
F_aF_g		1	Arbitrarily fixed	$f_{u,p}$		0.06	In house
$V_{central}$	L	65.4	See comment below	Kp_{liver}		0.6	In silico predicted
CL_{liver}	$L\cdot hour^{-1}$	70.4	See comment below				
			S-warfarin				
k_a	$hour^{-1}$	0.641	See comment below	$R_{B/P}$		0.63	In house
F_aF_g		1	(Holford, 1986)	$f_{u,p}$		0.012	In house
$V_{central}$	L	10.7	See comment below	Kp_{liver}		0.09	In silico predicted
CL_{liver}	$L\cdot hour^{-1}$	9.99	See comment below				
			R-warfarin				
k_a	$hour^{-1}$	0.493	See comment below	$R_{B/P}$		0.63	In house
F_aF_g		1	(Holford, 1986)	$f_{u,p}$		0.012	In house
$V_{central}$	L	8.93	See comment below	Kp_{liver}		0.09	In silico predicted
CL_{liver}	$L\cdot hour^{-1}$	7.23	See comment below				

Values of k_a, $V_{central}$, and CL_{liver} are estimated by fitting clinical data listed in Table 1.

Figure S1. Observed (Marker) and fitted (solid line) human plasma free fraction (A) and blood to plasma ratio (B). In subplot (B), blue and red represent measurement at 1 and 3 hours.

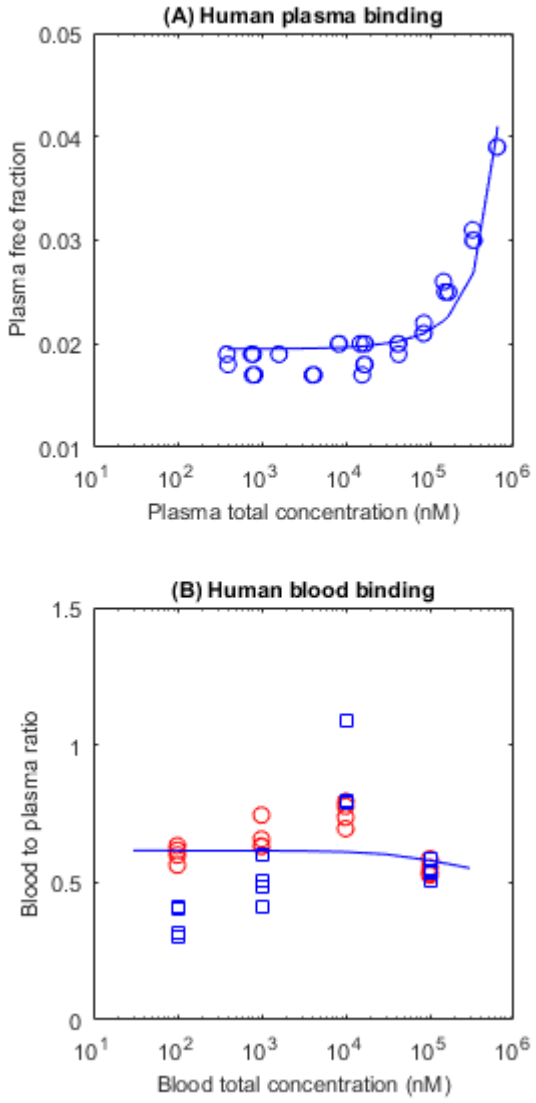

Figure S2. Observed (markers) and simulated (solid lines) induction effect of CYP3A4 (A and C) and 2B6 (B and D) due to bosentan. Subplots (A) and (B) represent activity measurements, while subplots (C) and (D) represent mRNA measurements. Red, blue, and black represent hepatocyte lots HC7-4, HH1025, and FOS.

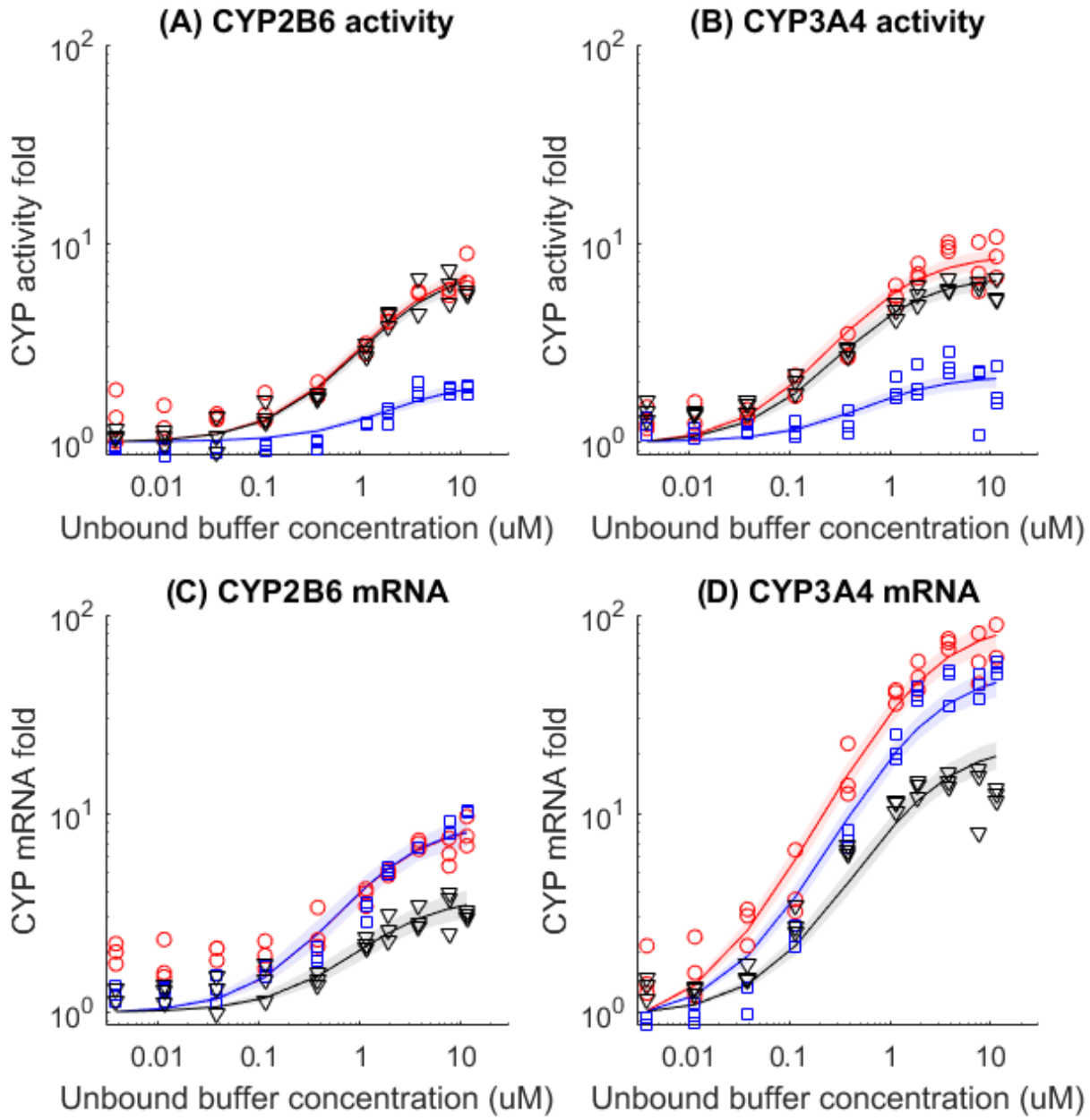

Reference

Alberty RA and Hammes GG (1958) Application of the Theory of Diffusion-controlled Reactions to Enzyme Kinetics. *The Journal of Physical Chemistry* **62:**154-159.

Dingemanse J, Bodin F, Weidekamm E, Kutz K, and van Giersbergen P (2002) Influence of food intake and formulation on the pharmacokinetics and metabolism of bosentan, a dual endothelin receptor antagonist. *J Clin Pharmacol* **42:**283-289.

Groer C, Busch D, Patrzyk M, Beyer K, Busemann A, Heidecke CD, Drozdzik M, Siegmund W, and Oswald S (2014) Absolute protein quantification of clinically relevant cytochrome P450 enzymes and UDP-glucuronosyltransferases by mass spectrometry-based targeted proteomics. *J Pharm Biomed Anal* **100:**393-401.

Holford NHG (1986) Clinical Pharmacokinetics and Pharmacodynamics of Warfarin. *Clinical Pharmacokinetics* **11:**483-504.

Nakamura K, Hirayama-Kurogi M, Ito S, Kuno T, Yoneyama T, Obuchi W, Terasaki T, and Ohtsuki S (2016) Large-scale multiplex absolute protein quantification of drug-metabolizing enzymes and transporters in human intestine, liver, and kidney microsomes by SWATH-MS: Comparison with MRM/SRM and HR-MRM/PRM. *Proteomics* **16:**2106-2117.

NDA-21-290 (2001) Clinical pharmacology and biopharmaceutics review. *Center for Drug Devaluation and Research, US Food and Drug Administration*.

Peters SA (2012) Appendices, in: *Physiologically-Based Pharmacokinetic (PBPK) Modeling and Simulations*, pp 407-421, John Wiley & Sons, Inc.

Rodgers T and Rowland M (2006) Physiologically based pharmacokinetic modelling 2: predicting the tissue distribution of acids, very weak bases, neutrals and zwitterions. *J Pharm Sci* **95:**1238-1257.

Shah DK and Betts AM (2012) Towards a platform PBPK model to characterize the plasma and tissue disposition of monoclonal antibodies in preclinical species and human. *J Pharmacokinet Pharmacodyn* **39:**67-86.

Turgeon ML (2017) *Clinical hematology: theory & procedures*. Wolters Kluwer, Philadelphia, PA.

van Giersbergen PL, Halabi A, and Dingemanse J (2002) Single- and multiple-dose pharmacokinetics of bosentan and its interaction with ketoconazole. *Br J Clin Pharmacol* **53:**589-595.

Volz AK, Krause A, Haefeli WE, Dingemanse J, and Lehr T (2017) Target-Mediated Drug Disposition Pharmacokinetic-Pharmacodynamic Model of Bosentan and Endothelin-1. *Clin Pharmacokinet*.

Weber C, Banken L, Birnboeck H, and Schulz R (1999a) Effect of the endothelin-receptor antagonist bosentan on the pharmacokinetics and pharmacodynamics of warfarin. *J Clin Pharmacol* **39:**847-854.

Weber C, Gasser R, and Hopfgartner G (1999b) Absorption, excretion, and metabolism of the endothelin receptor antagonist bosentan in healthy male subjects. *Drug Metab Dispos* **27:**810-815.

Weber C, Schmitt R, Birnboeck H, Hopfgartner G, Eggers H, Meyer J, van Marle S, Viischer HW, and Jonkman JH (1999c) Multiple-dose pharmacokinetics, safety, and tolerability of bosentan, an endothelin receptor antagonist, in healthy male volunteers. *J Clin Pharmacol* **39:**703-714.

Wrishko RE, Dingemanse J, Yu A, Darstein C, Phillips DL, and Mitchell MI (2008) Pharmacokinetic Interaction Between Tadalafil and Bosentan in Healthy Male Subjects. *The Journal of Clinical Pharmacology* **48:**610-618.

Yang J, Jamei M, Yeo KR, Tucker GT, and Rostami-Hodjegan A (2007) Prediction of intestinal first-pass drug metabolism. *Curr Drug Metab* **8:**676-684.

Yang X, Atkinson K, and Di L (2016) Novel Cytochrome P450 Reaction Phenotyping for Low-Clearance Compounds Using the Hepatocyte Relay Method. *Drug Metab Dispos* **44:**460-465.